

Paleoceanography and Paleoclimatology

RESEARCH ARTICLE

10.1029/2020PA003849

Special Section:

Special Collection to Honor the Career of Robert C. Thunell

Key Points:

- Terrestrial organic carbon is the dominant source of carbon to the SBB with deposition significantly increasing during flood events
- Episodic flood and turbidite remobilization events were responsible for over 25% of the OC buried in the SBB over the past 2,000 years
- Drought sedimentation had significantly lower sedimentation rates and had an *n*-alkane composition consistent with increased marine inputs

Supporting Information:

- Supporting Information S1
- Figure S1
- Figure S2
- Data Set S1

Correspondence to:

C. T. Sarno,
caitsarno@gmail.com

Citation:

Sarno, C. T., Benitez-Nelson, C. R., Ziolkowski, L. A., Hendy, I. L., Davis, C. V., Tappa, E. J., & Thunell, R. C. (2020). The impacts of flood, drought, and turbidites on organic carbon burial over the past 2,000 years in the Santa Barbara Basin, California. *Paleoceanography and Paleoclimatology*, 35, e2020PA003849. <https://doi.org/10.1029/2020PA003849>

Received 7 JAN 2020




Accepted 25 APR 2020

Accepted article online 7 JUN 2020

©2020. The Authors.

This is an open access article under the terms of the Creative Commons Attribution License, which permits use, distribution and reproduction in any medium, provided the original work is properly cited.

The Impacts of Flood, Drought, and Turbidites on Organic Carbon Burial Over the Past 2,000 years in the Santa Barbara Basin, California

Caitlyn T. Sarno¹ , Claudia R. Benitez-Nelson¹ , Lori A. Ziolkowski¹ , Ingrid L. Hendy² , Catherine V. Davis¹ , Eric J. Tappa¹ , and Robert C. Thunell^{1,3} 

¹School of the Earth, Ocean and Environment, University of South Carolina, Columbia, SC, USA, ²Department of Earth and Environmental Sciences, University of Michigan, Ann Arbor, MI, USA, ³Deceased July 30, 2018

Abstract Climate conditions and instantaneous depositional events can influence the relative contribution of sediments from terrestrial and marine environments and ultimately the quantity and composition of carbon buried in the sediment record. Here, we analyze the elemental, isotopic, and organic geochemical composition of marine sediments to identify terrestrial and marine sources in sediment horizons associated with droughts, turbidites, and floods in the Santa Barbara Basin (SBB), California, during the last 2,000 years. Stable isotopes ($\delta^{13}\text{C}$ and $\delta^{15}\text{N}$) indicate that more terrestrial organic carbon (OC) was deposited during floods relative to background sediment, while bulk C to nitrogen (C/N) ratios remained relatively constant (~ 10). Long-chain *n*-alkanes (C_{27} , C_{29} , C_{31} , and C_{33}), characteristic of terrestrial OC, dominated all types of sediment deposition but were 4 times more abundant in flood layers. Marine algae (C_{15} , C_{17} , and C_{19}) and macrophytes (C_{21} and C_{23}) were also 2 times higher in flood versus background sediments. Turbidites contained twice the terrestrial *n*-alkanes relative to background sediment. Conversely, drought intervals were only distinguishable from background sediment by their higher proportion of marine algal *n*-alkanes. Combined, our data indicate that 15% of the total OC buried in SBB over the past 2,000 years was deposited during 11 flood events where the sediment was mostly terrestrially derived, and another 12% of deep sediment OC burial was derived from shelf remobilization during six turbidite events. Relative to twentieth century river runoff, our data suggest that floods result in considerable terrestrial OC burial on the continental margins of California.

1. Introduction

Burial of organic carbon (OC) in marine sediments and coastal environments in particular transfers carbon from the short-term atmosphere-biosphere carbon cycle into semipermanent geological repositories. This carbon sequestration in the rock record ultimately influences global climate via the regulation of the greenhouse gas, carbon dioxide (Berner, 1982; Hedges & Keil, 1995; Martin et al., 1987; Sarmiento & Sundquist, 1992). The quantity and composition of OC buried in marine sediments is controlled by its source and transport to the deep sea. Thus, understanding the sources of OC buried in marine sediments (e.g., terrestrial vs. marine) provides insight into how coastal ecosystems influence carbon sequestration over geological time.

Oceanic primary productivity is hypothesized to account for 50% of the total global carbon fixed and approximately 10 times the carbon annually produced by fossil fuel burning (Schlesinger & Jiang, 1991; Smith & Hollibaugh, 1993). The coastal environment, while comprising a small proportion of the global oceans, plays a significant role in the carbon cycle due to its proximity to river runoff and nutrient-rich waters that increase marine primary productivity (Bianchi, 2011; Muller-Karger et al., 2005). Rivers carry significant terrestrial OC to the ocean, where it may be remineralized in the water column or buried in marine sediments (Hedges & Keil, 1995). Small mountain river systems, such as those on the Southern California Margin, are an especially effective mechanism of OC burial. These systems are characterized by episodic discharge events, and the sediments are more likely to survive coastal processing and reach the deep sea due to the characteristically narrow continental shelves of the margin (Masiello & Druffel, 2001). Rapid sediment deposition events, such as turbidity currents (downslope remobilization of sediments) and floods, rapidly

transport OC to low-oxygen seafloor sediments where remineralization is less efficient, thus facilitating the burial of significant quantities of OC (Burdige, 2006).

Santa Barbara Basin (SBB), California, is an optimal environment for paleoclimate reconstructions due to its suboxic bottom water and high sedimentation rate (Hendy et al., 2013; Soutar et al., 1977). This creates an ideal location to examine the character and efficiency of carbon sequestration in a coastal environment. Here, we measured total OC (TOC), total nitrogen (TN), molar C/N ratios, $\delta^{13}\text{C}$ and $\delta^{15}\text{N}$ isotopes, and *n*-alkane biomarkers in a well-dated sediment core (Hendy et al., 2013) to elucidate the source of organic matter (OM) to marine sediments during episodic rapid deposition events (e.g., floods and turbidites) and lower sedimentation intervals (i.e., droughts). Understanding the composition of OM transported by different mechanisms and deposited under different environmental conditions provides information regarding how coastal ecosystems influence carbon sequestration over decadal to geologic timescales.

1.1. Study Site

Southern California often experiences floods and droughts due to its Mediterranean climate and in response to the El Niño–Southern Oscillation (ENSO) and Pacific Decadal Oscillation (PDO) (Hendy et al., 2015; Schimmelmann et al., 2003; Soutar & Crill, 1977). During the warm phases of ENSO and PDO, precipitation and river discharge increase, supplying more terrestrial sediment to the California coast (Hendy et al., 2015; Ropelewski & Halpert, 1989; Warrick & Farnsworth, 2009). In addition, these warm phases are associated with increased transport of warm, nutrient-depleted water from the subtropics, reducing marine productivity (Bograd & Lynn, 2001; Chavez, 1996). The West Coast of the United States is also vulnerable to extreme floods, termed megafloods (Dettinger & Ingram, 2013). These megafloods are caused by excessive rain from atmospheric rivers that may be further enhanced by ENSO (Dettinger & Ingram, 2013). Atmospheric rivers often occur on shorter timescales and are responsible for delivering 30–50% of the annual precipitation to California (Dettinger & Ingram, 2013).

The SBB is located off the coast of Southern California where it is bounded by mountains to the north, islands to the south, and sills to the east and west that impede circulation in the deep basin (Figure 1). Restricted circulation reduces the oxygen supply to bottom waters, creating a suboxic environment at a depth below 480 m (Li et al., 2009). The resulting anoxic sediment minimizes bioturbation creating high-resolution sedimentary records (Hendy et al., 2013; Hülsemann & Emery, 1961). Highly refined age models have been developed for SBB sediments; thus, there is an opportunity to examine episodic regional climate events, such as floods and droughts, over thousands of years (Hendy et al., 2015; Schimmelmann et al., 2003; Soutar et al., 1977).

Annually, there are two compositionally different periods of sedimentation in the SBB. During the winter, the North Pacific High and the Jet Stream migrate south, strengthening the Aleutian Low causing mild, wet, and stormy conditions (Barron et al., 2010; Dorman & Winant, 2000). These wet conditions increase terrestrial input via river discharge and sediment transport to the basin (Hendy et al., 2015; Hülsemann & Emery, 1961; Thunell et al., 1995). During the spring/summer, the North Pacific High produces strong northerly winds that induce coastal upwelling in California and support high biological productivity (Hendy et al., 2013; Hülsemann & Emery, 1961; Thunell et al., 1995). As a result, marine biogenic sediment, dominated by diatoms (biogenic silica) and foraminifera (calcium carbonate), ultimately reach the basin bottom and are buried (Barron et al., 2010). Biogenic sediment can enhance clay sedimentation by flocculation of clays onto marine snow (Deuser et al., 1983; Thunell et al., 1995). Additional sources of sedimentary material in the spring/summer may include benthic bacterial mats (e.g., *Beggiatoa*) that form after winter terrestrial inputs (Soutar & Crill, 1977), or in response to annual oxygenation of the basin during upwelling periods (Bograd et al., 2002; Reimers et al., 1990). Together, one terrestrial-rich and one biogenic-rich sediment laminae represent a single year (Hendy et al., 2015; Soutar & Crill, 1977; Thunell et al., 1995).

In addition to the annual lamina of terrestrial and marine sediment, this core also contained lamina consistent with floods, droughts, and turbidites. ENSO and PDO change precipitation patterns that produce floods (warm phase) and droughts (cold phase) in the SBB region (Chavez, 1996; Graham et al., 2007; Schimmelmann et al., 2003). During a flood event, there is rapid transport of lithogenic sediment to the basin, and annual laminae are replaced by a thick, gray flood layer (Barron et al., 2015). Turbidites are also present, distinctive from flood layers in that they transport sediment from the shelf into the deeper basin (Du

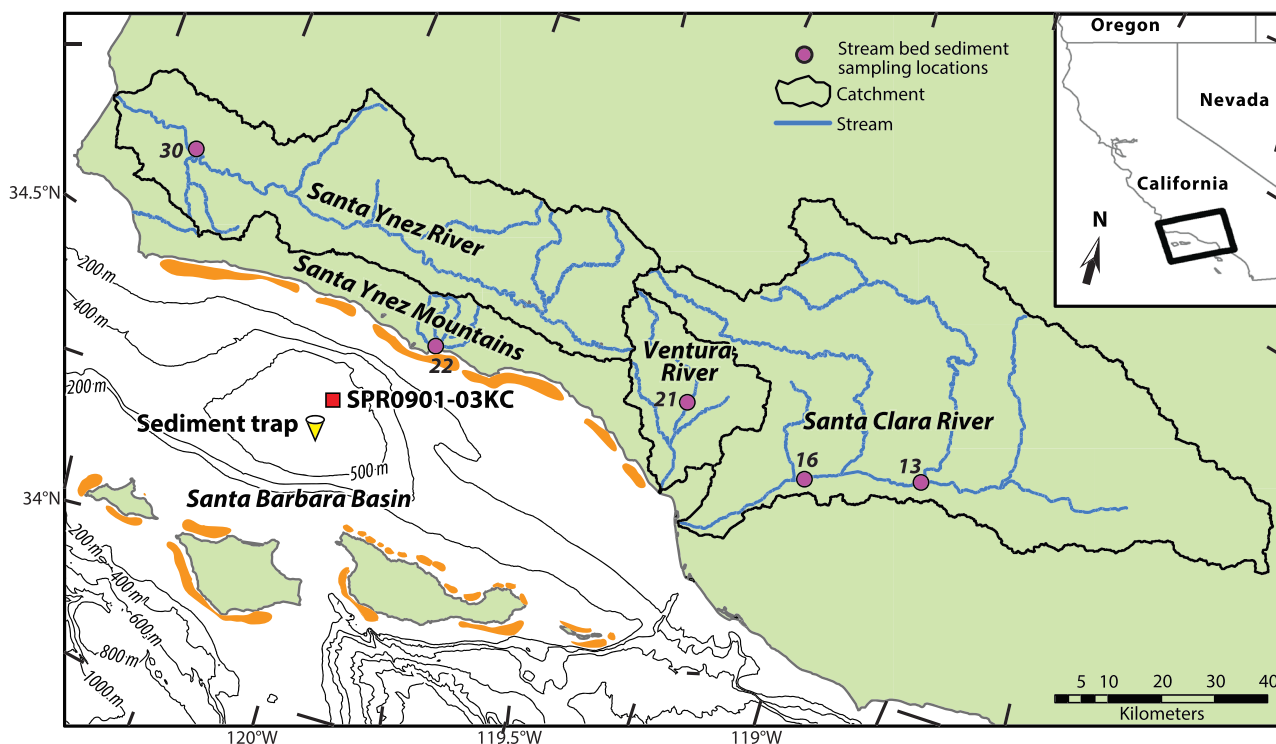


Figure 1. Map of the Santa Barbara Basin (SBB). The sediment core is labeled by the red square ($34^{\circ}16.99'N$, $120^{\circ}2.41'W$), the sediment trap is denoted by the yellow triangle ($34^{\circ}14'N$, $120^{\circ}02'W$), and the river collection sites are marked by the purple circles (see Napier et al., 2019): Santa Clara River, Locations 13 ($34^{\circ}23.10'N$, $118^{\circ}47.22'W$) and 16 ($34^{\circ}20.70'N$, $119^{\circ}01.46'W$); Ventura River, Location 21 ($34^{\circ}25.20'N$, $119^{\circ}17.94'W$); and the Santa Ynez River, Locations 22 ($34^{\circ}24.60'N$, $119^{\circ}49.74'W$) and 30 ($34^{\circ}38.40'N$, $120^{\circ}24.54'W$). Kelp beds are denoted by shaded orange regions in the nearshore environment of the SBB (Schimmelmann & Tegner, 1991).

et al., 2018). Turbidites are visually distinct from flood deposits as they are characterized by an olive coloration and larger grain size (Hendy et al., 2013; Schimmelmann et al., 1998).

1.2. Geochemical Tools

The impacts of episodic flooding, turbidite events, and prolonged drought on carbon burial in the SBB are poorly understood. This study utilizes stable isotopes ($\delta^{13}C$ and $\delta^{15}N$) of bulk sediments, TOC and TN concentrations, and *n*-alkane lipid biomarker concentrations to determine sediment composition from flood and turbidite events, drought periods, and background sediment. Background sediments were selected based on the absence of properties characteristic of floods, turbidites, or droughts. Carbon to nitrogen (C/N) ratios provide a broad view of OM source, where C/N molar ratios >20 are indicative of the structural material required by land plants (Hedges et al., 1986). However, C/N ratios are often imprecise due to the mixing of multiple sediment inputs (rivers, marine algae, vascular plants, etc.). As such, OM stable isotopes are also used to determine sediment source. In terrestrial environments, the isotopic composition of plants is usually depleted in the heavier isotopes (i.e., $\delta^{13}C_{\text{terrestrial}} = -27\text{‰}$ and $\delta^{15}N_{\text{terrestrial}} = 2\text{‰}$), while marine sources tend to have a higher isotopic signal ($\delta^{13}C_{\text{marine}} = -20\text{‰}$ and $\delta^{15}N_{\text{marine}} = 10\text{‰}$) (Meyers, 1994; Sweeney & Kaplan, 1980).

While C and N isotopes may distinguish OM source (marine vs. terrestrial), these isotopes also undergo additional fractionation processes both in the water column and on land. Surface water entering SBB during the summer and fall flows northward from the Eastern Tropical North Pacific (Bray et al., 1999) where denitrification results in higher $\delta^{15}N$ by utilizing nitrate as a terminal electron acceptor in respiration in place of oxygen (Brandes et al., 2003; Davis et al., 2019; Emmer & Thunell, 2000; Sigman et al., 2003; Voss et al., 2001). Denitrification raises the $\delta^{15}N$ signal as the lighter nitrogen isotope is preferentially utilized to form nitrogen gas, leaving behind an enriched pool of nitrogen (Cline & Kaplan, 1975). It should be noted that additional denitrification sometimes occurs within the suboxic waters and anoxic sediments of the SBB

(Sigman et al., 2003; Thunell, 2003). In spring, strong winds stimulate upwelling of nutrient-enriched waters, potentially resulting in sinking OM lower in $\delta^{15}\text{N}$ as organisms preferentially utilize the lighter isotopes of N in nitrate. This leaves the remaining water enriched in ^{15}N until complete nitrate utilization occurs (Davis et al., 2019). As waters become increasingly nutrient depleted, organisms reduce their discrimination against specific isotopes during uptake and sinking OM increasingly contains higher $\delta^{15}\text{N}$ (Altabet et al., 1999; Cline & Kaplan, 1975). Once complete nitrate utilization occurs, the $\delta^{15}\text{N}$ of OC reflects that of the surrounding water. Carbon isotope signatures are equally complex as light and heavy isotopes are differentially fractionated by C_3 and C_4 metabolic processes, making it difficult to distinguish terrestrial sources from marine algae if the terrestrial source is composed of high proportions of C_4 plants (Meyers, 1994).

Given the multitude of controls on the isotopic composition of sediment, we also assessed the utility of *n*-alkane biomarkers to distinguish sediment source (Blumer & Clark, 1967). Biomarkers are molecular compounds characteristic of a specific organism under a particular set of environmental conditions. Here, we focused on *n*-alkanes as they are generally unreactive and degrade slowly over time, and their chain length typically reflects source. Terrestrial vegetation is characterized by long-chain *n*-alkanes (C_{27} , C_{29} , C_{31} , and C_{33}), which are utilized for protection and support in leaf waxes (Ficken et al., 2000; Meyers, 2003). On the other hand, marine phytoplanktons are characterized by short-chain *n*-alkanes (C_{15} , C_{17} , and C_{19}) and marine macrophytes by midlength chain *n*-alkanes (C_{21} , C_{23} , and C_{25}) (Ficken et al., 2000; Meyers, 2003). By measuring the distribution of *n*-alkanes in sediment, the relative contribution from marine and terrestrial sources can be determined.

The objective of this study was to analyze the TOC, TN, the C/N ratio, $\delta^{13}\text{C}$ and $\delta^{15}\text{N}$ isotopes, and *n*-alkane biomarkers of a well-dated sediment core collected from the center of SBB (previously age dated by Hendy et al., 2013) to elucidate the source of OM to marine sediments during episodic events (e.g., floods and turbidites) and under different climate states (e.g., droughts). Understanding the composition of OC deposited in these sediments by different processes and under various climate conditions provides information regarding how coastal ecosystems may influence global C sequestration.

2. Methods

2.1. Collection and Dating

A sediment core (SPR0901-03KC; $34^{\circ}16.99'\text{N}$, $120^{\circ}2.41'\text{W}$, Figure 1) was collected from the SBB in January 2009 at a water depth of 586 m (Hendy et al., 2013). Floods, turbidites, and droughts were identified from scanning X-ray fluorescence (SXRF) elemental analyses (Hendy et al., 2015; Heusser et al., 2015). Flood sediments were composed of high concentrations of lithogenic elements such as titanium (Ti), potassium (K), iron (Fe), and calcium (Ca) and had a high clay content. Drought sediments were composed of low lithogenic element concentrations. Turbidites were identified by their olive homogenous coloration and larger grain size (Du et al., 2018; Hendy et al., 2013; Schimmelmann et al., 1998). Following SXRF, the core was sampled at 2 mm intervals and oven dried. An age model was developed using a combination of ^{14}C dating of planktonic foraminiferal carbonates and laminae counts (Hendy et al., 2013; Wang, Hendy, & Thunell, 2019). The age-depth model was generated using Bacon 2.2 (Blaauw & Christen, 2011; Du et al., 2018), where ^{14}C ages were converted to calendar ages using the Marine13 calibration curve (Reimer et al., 2013) with variable reservoir ages from Hendy et al. (2013).

Terrestrial end members were defined using river sediment previously collected from dry streambeds during the drought of 2013–2016 (Napier et al., 2019) (Figure 1). River sediments from five locations were analyzed: The Santa Clara River was sampled at Locations 13 ($34^{\circ}23.10'\text{N}$, $118^{\circ}47.22'\text{W}$) and 16 ($34^{\circ}20.70'\text{N}$, $119^{\circ}01.46'\text{W}$); the Ventura River was sampled at Location 21 ($34^{\circ}25.20'\text{N}$, $119^{\circ}17.94'\text{W}$); and the Santa Ynez River was sampled at Locations 22 ($34^{\circ}24.60'\text{N}$, $119^{\circ}49.74'\text{W}$) and 30 ($34^{\circ}38.40'\text{N}$, $120^{\circ}24.54'\text{W}$) as described in Napier et al. (2019). The macrophyte end member was defined by a sample of *Macrocystis pyrifera* that was collected from Coal Oil Point in June 2018. Samples were shipped to the University of South Carolina where they were freeze dried and ground prior to analysis.

Sediment traps were utilized to compare sediment core events, such as paleofloods, to modern-day flood and background sedimentation. The sediment traps were deployed in the center of the SBB ($34^{\circ}14'\text{N}$, $120^{\circ}02'\text{W}$; Figure 1) at a depth of 500 m in 1993 and continue to the present day (Thunell, 1998). Sediment trap flood

samples were selected from the 1997–1998 El Niño flood collected in March–April 1998 (Bograd & Lynn, 2001). Sediment trap samples reflecting background conditions were selected from November 2000 and November 2001 to avoid years associated with flooding, turbidites, or drought.

2.2. TOC, TN, and Isotopic Measurements

For the sediment core, the weight percent TOC (%TOC) and TN (%TN) were measured on Costech ECS 4010 Elemental Analyzer at University of Michigan using the methods of Wang, Hendy, and Thunell (2019). For the sediment traps, rivers, and kelp samples, the %TOC and %TN were measured on a PerkinElmer 2400 CHNS Elemental Analyzer. The standard deviation of TOC and TN measurements for standard replicates was 0.03% and 0.04%, respectively. For OC analyses (TOC and $\delta^{13}\text{C}$), inorganic C was removed by acidifying 0.5 mg of sediment with 6 ml of 1 M phosphoric acid, sonicating for 5 min, and filtering onto a precombusted GF/F. The filters were dried overnight, folded into 3.0 cm tin disk, and pelletized for analysis. For isotopic analysis of C and N, all samples were combusted in a Eurovector Elemental Analyzer connected to an Elementar Isoprime IRMS. Reference materials for ^{13}C were USGS-24, USGS-40, and sucrose. Reference materials for ^{15}N were IAEA-N1, N2 (ammonium sulfates) and USGS-40. Isotopic measurements are given in reference to a standard; $\delta^{13}\text{C}$ was reported relative to Vienna Pee Dee Belemnite (VPDB) with a standard deviation of 0.15‰, and $\delta^{15}\text{N}$ was reported relative to atmospheric nitrogen (0‰) with standard deviation of 0.04‰.

2.3. *n*-Alkane Analyses

Approximately 2 g of homogenized and dried sediment or kelp was used for lipid extraction. Given the large amount of material needed, multiple core intervals of similar isotopic nitrogen signatures were pooled together for extraction, encompassing ~1 year for flood and turbidite samples and ~8 years for background and drought samples. Lipids were extracted in triplicate by sonicating for 30 min in 50 ml of a 9:1 dichloromethane/methanol (DCM/MeOH) solution and filtering through a GF/F. The extract was concentrated to 2 ml via evaporation under ultrahigh purity nitrogen gas. Sulfur was removed from samples by adding ~500 mg activated copper and allowing samples to stand overnight.

The *n*-alkanes were separated from the total lipid extract with silica gel column chromatography. Briefly, the column was packed with 7 cm of silica gel in DCM and 1 cm of anhydrous sodium sulfate to prevent aqueous contamination. The column was made with DCM to minimize contamination that arose from hexane extracting atmospheric contaminants. To switch to a hexane column, the column was loaded with 40 ml of hexane before loading the sample. Once the sample was added, the first fraction (40 ml hexane) was collected for hydrocarbon analysis. This hydrocarbon fraction was evaporated to 500 μl under ultrahigh purity nitrogen gas and analyzed with a GC/MS. The remaining fractions were stored for future analysis of ketones/esters (40 ml 4:1 hexane/DCM), alcohols (40 ml 9:1 DCM/acetone), and fatty acids (40 ml 12:12:1 DCM/MeOH/formic acid).

Identification and quantification of *n*-alkanes were conducted using an Agilent 7890B/5977A GC/MS with HP-5MS column outfitted with UHP helium as a carrier gas. One microliter of sample was injected into the GC/MS on splitless mode. The initial column temperature was 100°C, increased at a rate of 8°C min^{-1} until 300°C, and remained at 300°C for 23 min. *n*-Alkanes were detected utilizing scanning ion monitoring (SIM) targeting the m/z ion 71 and identified using external standards of known retention times and by analysis of the SIM chromatograms. *n*-Alkane concentrations were determined using external standards (C_{20} , C_{24} , C_{26} , and C_{30}) and extrapolating the slopes for the other *n*-alkane chain lengths. Blanks were processed with every batch of seven samples.

A carbon preference index (CPI) was utilized as a proxy for fresh OC (Bray & Evans, 1961). In this study, a modified CPI equation (Bray & Evans, 1961; Pearson & Eglinton, 2000; Scalan & Smith, 1970) was used to encompass the entire spectrum of contributing *n*-alkanes (Equation 1).

$$\text{CPI} = \frac{\text{C}_{13} + \text{C}_{15} + \text{C}_{17} + \text{C}_{19} + \text{C}_{21} + \text{C}_{23} + \text{C}_{25} + \text{C}_{27} + \text{C}_{29} + \text{C}_{31} + \text{C}_{33}}{\text{C}_{14} + \text{C}_{16} + \text{C}_{18} + \text{C}_{20} + \text{C}_{22} + \text{C}_{24} + \text{C}_{26} + \text{C}_{28} + \text{C}_{30} + \text{C}_{32}} \quad (1)$$

The numerator in this equation is the sum of the concentration ($\mu\text{g g}^{-1}$ OC) of all odd chain *n*-alkanes from 13 to 33 carbon atoms in length (C_{13} , C_{15} , etc.), and the denominator is the sum of the concentration of all

Table 1

Average Relative Abundance of Total Organic Carbon (TOC), and Total Nitrogen (TN) and Molar C/N Ratios and Isotopic Composition in Santa Barbara Basin Sediments and Sediment End Members

	Background	Drought	Flood	Turbidite	Kelp	Sediment trap background	Sediment trap flood
	<i>n</i> = 33	<i>n</i> = 25	<i>n</i> = 58	<i>n</i> = 34	<i>n</i> = 1	<i>n</i> = 2	<i>n</i> = 2
TOC (wt %)	3.70 ± 0.31	3.90 ± 0.25	2.13 ± 0.53	2.98 ± 0.23	13.79	3.79 ± 0.25	3.53 ± 1.87
TN (wt %)	0.41 ± 0.04	0.44 ± 0.03	0.22 ± 0.06	0.33 ± 0.03	1.04	0.48 ± 0.07	0.52 ± 0.31
C/N	10.67 ± 0.47	10.34 ± 0.28	11.45 ± 1.03	10.63 ± 0.55	15.47	9.27 ± 0.75	8.12 ± 0.67
δ ¹³ C (‰)	−21.9 ± 0.09	−21.98 ± 0.09	−24.34 ± 0.84	−22.5 ± 0.21	−14.73	−21.01 ± 0.64	−22.12 ± 0.16
δ ¹⁵ N (‰)	7.54 ± 0.20	7.88 ± 0.09	6.26 ± 0.84	7.59 ± 0.21	9.79	7.87 ± 0.19	6.62 ± 0.21

even chain *n*-alkanes from 14 to 32 carbon atoms in length (C₁₄, C₁₆, etc.). Previous work has shown that a higher CPI indicates a greater contribution from fresh OC sources (Bray & Evans, 1961). A lower CPI and increased abundance of even chain *n*-alkanes were derived from bacterial degradation and petroleum (Bray & Evans, 1961; Grimalt et al., 1985).

The burial rates of OC (Equation 2) and each type of *n*-alkane (Equation 3) were determined for each type of sedimentation (flood, turbidites, droughts, and background) over the past 2,000 years:

$$\text{OC Burial Rate (g cm}^{-1} \text{ kyr}^{-1}) = \text{MAR (g cm}^{-1} \text{ kyr}^{-1}) * \text{TOC} \left(\frac{1}{100} \right), \quad (2)$$

$$n - \text{Alkanes Burial Rate} (\mu\text{g cm}^{-1} \text{ kyr}^{-1}) = \text{OC Burial Rate} * n - \text{alkane} \left(\frac{\mu\text{g}}{\text{gTOC}} \right). \quad (3)$$

The above equations utilized sediment mass accumulation rate (MAR; g cm^{−2} year^{−1}; Equation 4), %TOC (1/100), and *n*-alkane concentration (μg g^{−1} OC). The *n*-alkane burial was separated into three categories based on chain length (algal, macrophyte, or terrestrial). Organic C and *n*-alkane burial during each type of sedimentation were compared to the TOC and *n*-alkanes buried over the past 2,000 years (Equation 5).

$$\text{MAR (g cm}^{-1} \text{ kyr}^{-1}) = \text{Linear sedimentation rate (cm kyr}^{-1}) * \text{Dry Bulk Density (g cm}^{-3}), \quad (4)$$

$$\% \text{OC Buried} = \frac{\text{OC Burial of Sedimentation Type (i.e., flood, drought, turbidite, or background)}}{\text{Sum of OC Burial for Every Sedimentation Type}} \times 100. \quad (5)$$

2.4. Statistical Analysis

Significant differences between samples were determined using a one tailed Student's *t* test assuming unequal variances where $\alpha < 0.05$. These statistical analyses allowed for gross characterization of events (i.e., flood vs. background). While this study may suggest transport mechanisms to the ocean floor, we did not account for any transformations that may have occurred in the water column. We also assume that there was no preferential degradation of specific *n*-alkanes within the water column or sediment (see section 4.4).

3. Results

Flood events are identified in the sediment core by SXRF as having high concentrations of lithogenic-associated elements, Ti and Fe, and low concentrations of the biogenic-associated element, Ca (Du et al., 2018; Hendy et al., 2015). Drought intervals are identified by low concentrations of lithogenic elements and high concentrations of biogenic Ca and Si (Hendy et al., 2015). Turbidite sediment is visually characterized by a homogenous olive coloration and larger grain size and is derived from turbidity currents

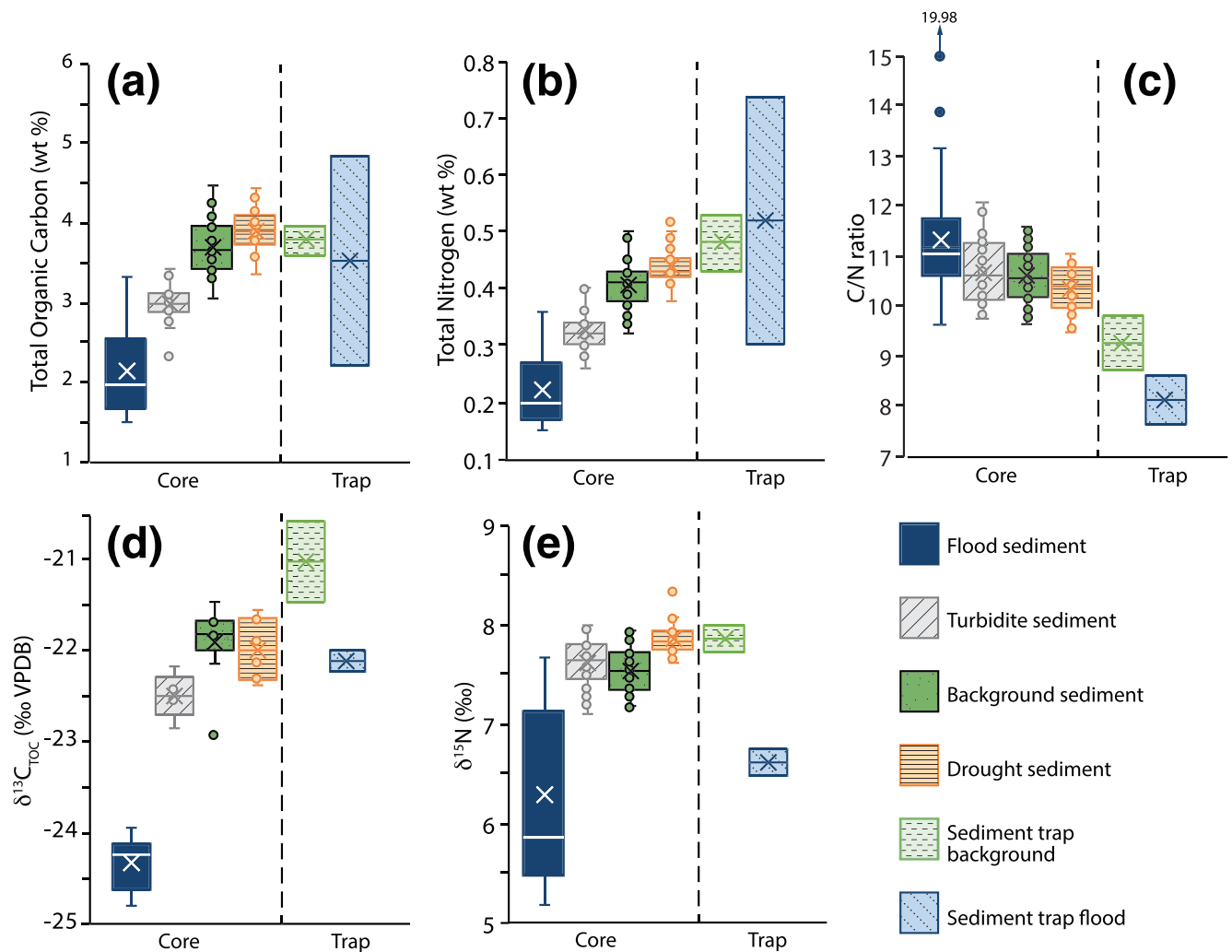


Figure 2. Box plot comparisons of composition by sediment type: flood (dark blue solid box), turbidites (pale gray diagonal striped box), background (dark green speckled box), and drought (orange horizontal striped box) sediments relative to sediment trap background (pale green-dashed box) and flood (pale blue-dashed horizontal striped box) for (a) total organic carbon (wt %), (b) total nitrogen (wt %), (c) C/N ratio, (d) $\delta^{13}\text{C}$ (‰ SMO), and (e) $\delta^{15}\text{N}$ (‰). Within each box, the line is the median, the X is the mean, and points outside of the boxes (greater than 1.5 quartiles) are outliers.

stimulated by mass failure on the basin slope (Du et al., 2018; Hendy et al., 2015; Rack & Merrill, 1995; Schimmelfmann et al., 1998).

3.1. TOC, TN, C/N, and Isotopic Results

Flood sediment has significantly lower average TOC, TN, $\delta^{13}\text{C}$ and $\delta^{15}\text{N}$ relative to background sediment ($p < 0.001$), and a significantly higher molar C/N ratio ($p < 0.001$; Table 1 and Figure 2). These results are in excellent agreement with SXRF-derived trace element measurements used to identify floods (Hendy et al., 2015) (Figure 3). Turbidites contain a mixture of flood and background sediment characteristics, with TOC and TN concentrations significantly different from flood and background sedimentation ($p < 0.001$). Turbidites have C/N ratios and $\delta^{15}\text{N}$ signatures similar to background sediment, while the turbidite $\delta^{13}\text{C}$ signature is significantly lower ($p < 0.001$). Drought intervals are nearly indistinguishable from background sediment with regard to TOC, TN, and C/N ratios.

Sediment trap samples collected during and after the 1997–1998 El Niño are analyzed to constrain recent flood and background source signatures in the SBB. Sediment trap TOC and TN concentrations are highly variable, particularly during flood periods, and both flood and background sediment trap material are significantly higher than those measured in flood sediments. Flood sediment trap C/N is significantly lower than

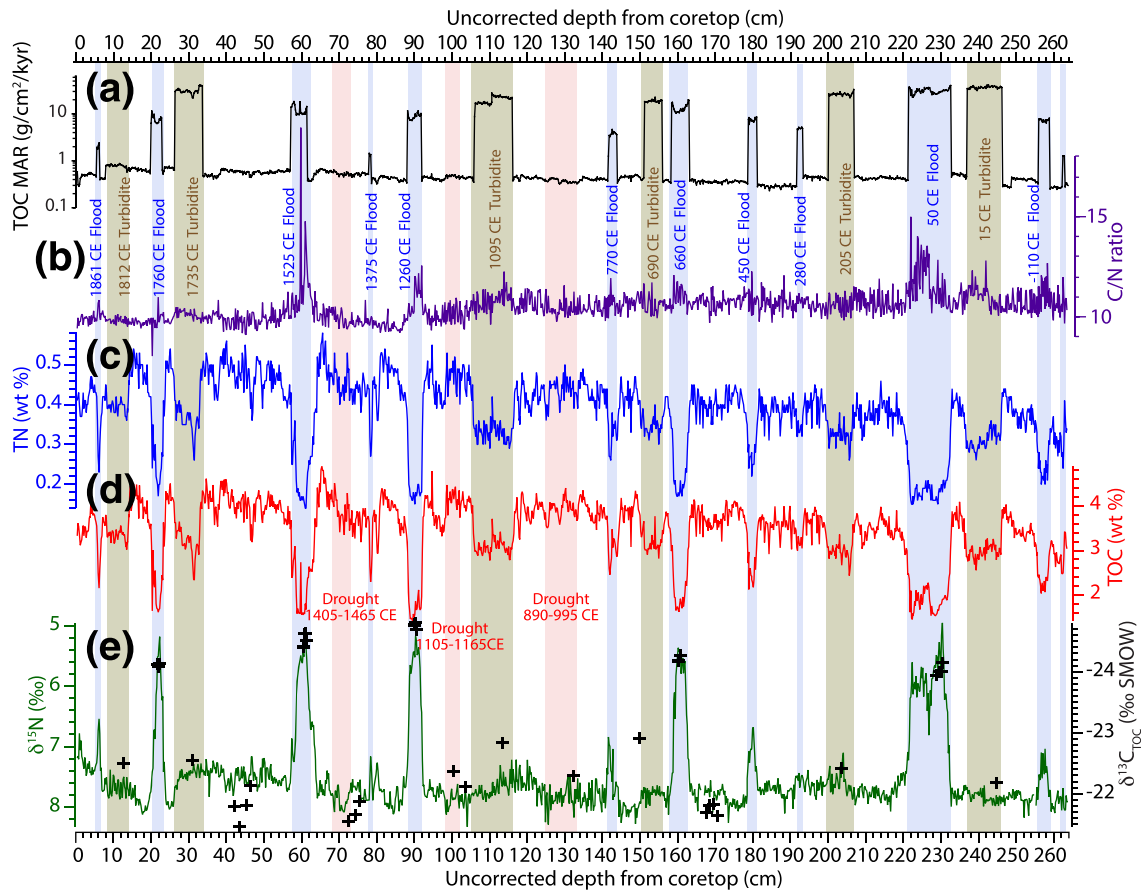


Figure 3. Uncorrected depth profiles spanning the past 2,000 years from the SBB sediment record. (a) Total organic carbon (TOC) mass accumulation rates (MAR) ($\text{g cm}^{-2} \text{ kyr}^{-1}$; black line), (b) molar C/N ratio (purple line), (c) total nitrogen (TN) (wt %; blue line), (d) total organic carbon (TOC) (wt %; red line), and (e) $\delta^{13}\text{C}$ (‰ SMOW; black crosses) and $\delta^{15}\text{N}$ (‰; green line) vary during instantaneous events, such as flooding (blue-shaded bars), turbidites (tan-shaded bars) (Du et al., 2018), and droughts (red-shaded bars) (Heusser et al., 2015).

flood sediment ($p < 0.01$), and background sediment trap C/N is lower than that measured in core background sediment ($p = 0.06$). The $\delta^{13}\text{C}$ signatures of both background and flood sediment trap material are similar to background sediments. In contrast, the $\delta^{15}\text{N}$ signature of the flood sediment trap is

Table 2

Relative Concentrations of Total Organic Carbon (TOC), Total Nitrogen (TN), *n*-Alkanes, C/N Ratios, and Isotopic Composition of Bed Load Sediments in Rivers Draining Into the Santa Barbara Basin

	Location number ^a					Average river sediment
	13	16	21	22	30	
	Santa Clara River	Santa Clara River	Ventura River	Santa Ynez River	Santa Ynez River	
Latitude, longitude	34°23.10'N, 118°47.22'W	34°20.70'N, 119°01.46'W	34°25.20'N, 119°17.94'W	34°24.60'N, 119°49.74'W	34°38.40'N, 120°24.54'W	—
C ₂₅ ($\mu\text{g g}^{-1}$ OC)	6	BDL	BDL	7	12	5 ± 5
Terrestrial C ₂₇ , C ₂₉ , and C ₃₁ ($\mu\text{g g}^{-1}$ OC)	147	146	820	118	192	285 ± 269
TOC	2.68	0.43	0.87	2.13	1.15	1.45 ± 0.93
TN	0.25	0.07	0.12	0.19	0.14	0.15 ± 0.07
C/N	12.51	7.17	8.46	13.08	9.58	10.16 ± 2.56
$\delta^{13}\text{C}$ (‰)	-24.77	-31.53	-22.80	-27.10	-24.05	-26.05 ± 3.44
$\delta^{15}\text{N}$ (‰)	7.00	8.51	4.41	6.28	6.30	6.50 ± 1.48

^a Sample location description in Napier et al. (2019).

Table 3
Concentration of *n*-Alkanes in Santa Barbara Basin Sediments and End Members

	Background	Flood	Turbidite	Drought	Kelp	Sediment trap background	Sediment trap flood	Rivers
	<i>n</i> = 7	<i>n</i> = 12	<i>n</i> = 6	<i>n</i> = 5	<i>n</i> = 1	<i>n</i> = 2	<i>n</i> = 2	<i>n</i> = 5
CPI	2.41 ± 1.90	3.47 ± 1.67	4.08 ± 4.79	2.78 ± 2.45	2.12	5.96 ± 2.34	3.33 ± 1.12	Only odds
Algal C ₁₅ , C ₁₇ , and C ₁₉ (μg g ⁻¹ OC)	6 ± 5	11 ± 13	7 ± 3	7 ± 7	16	20 ± 22	27 ± 11	BDL
Macrophyte C ₂₁ and C ₂₃ (μg g ⁻¹ OC)	2 ± 3	5 ± 7	3 ± 3	4 ± 6	7	5 ± 7	BDL	BDL
Terrestrial C ₂₇ , C ₂₉ , and C ₃₁ (μg g ⁻¹ OC)	23 ± 13	70 ± 42	23 ± 14	15 ± 7	BDL	30 ± 7	40 ± 33	285 ± 300

indistinguishable from that measured in flood sediments, again supporting the use of δ¹⁵N as a tracer of flood events.

Kelp is measured to constrain the inputs of macrophytes to the basin, while sediment from each of the rivers is measured to constrain the terrestrial end member. Kelp is characterized by a higher C/N ratio, δ¹³C, and δ¹⁵N (Table 1). While the C/N ratios for each river are similar, the isotopic composition is more variable; δ¹³C ranges from -31.53‰ to -22.80‰, and δ¹⁵N ranges from 4.41‰ to 8.51‰ (Table 2). Nonetheless, average δ¹³C and δ¹⁵N signatures of river sediments are consistent with those measured in flood sediments.

3.2. *n*-Alkanes

The *n*-alkane composition of kelp is used to characterize the macrophyte end member, while the terrestrial end member is constrained using river samples collected during a drought period. During a drought, riverine sediment is likely dominated by terrestrial vegetation adapted to low water conditions as riverine algae are minimal due to dry streambeds. As such, this end member may not be fully representative of the terrestrial end member during floods. River sediments contain 94–100% long-chain *n*-alkanes and range in concentration from 118 to 820 μg g⁻¹ OC (Table 2). These river sediments are in agreement with previously reported terrestrial *n*-alkane compositions (Ficken et al., 2000; Meyers, 2003). Kelp contains midchain *n*-alkanes, C₂₁ and C₂₃, but did not contain C₂₅. However, the Santa Clara and Santa Ynez Rivers did contain the *n*-alkane, C₂₅, most likely due to river macrophytes that the Ventura River lacked (Table 2). We therefore exclude C₂₅ from our marine macrophyte end member analyses to remove the potential freshwater influence.

Flood events are characterized by higher total *n*-alkane concentrations and greater changes in the relative *n*-alkane composition. Terrestrial *n*-alkane (C₂₇, C₂₉, C₃₁, and C₃₃) concentrations in flood sediments are significantly higher than those measured in background sediments (81% vs. 75% of total *n*-alkanes, *p* = 0.001) (Table 3 and Figures 4–6). Flood events are also characterized by approximately double the concentration of

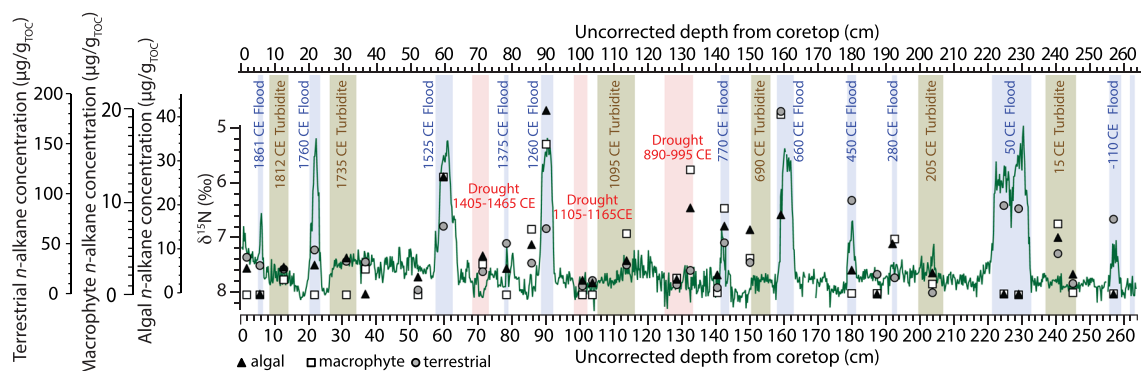


Figure 4. Comparison of 2,000 years of δ¹⁵N (‰; green line) and *n*-alkane concentrations normalized to TOC (μg g⁻¹ TOC) by depth in sediment core. The concentration of terrestrial (C₂₇, C₂₉, C₃₁, and C₃₃; gray circles), macrophyte (C₂₁ and C₂₃; white squares), and algal (C₁₅, C₁₇, and C₁₉; black triangles) *n*-alkanes varies during instantaneous events such as flooding (blue bars) and turbidites (tan bars) (Du et al., 2018) as well as during drought intervals (pink bars) (Heusser et al., 2015). *n*-Alkane concentrations depicted as 0 are below detection limit (BDL) of 0.5 mg L⁻¹ in hexane on the GC/MS.

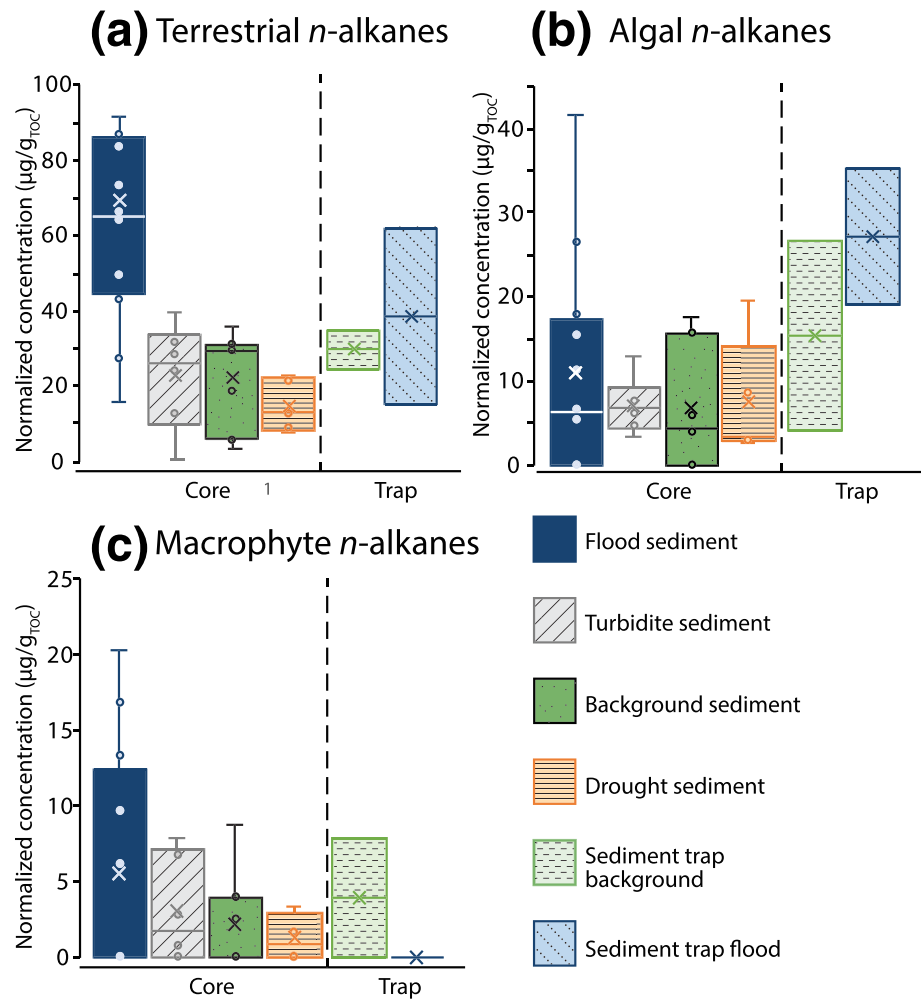


Figure 5. Box plot comparison of normalized concentrations ($\mu\text{g g}^{-1}$ TOC) of *n*-alkane source by sediment type: flood (dark blue solid box), turbidites (pale gray diagonal striped box), background (dark green speckled box), and drought (orange horizontal striped box) sediments relative to sediment trap background (pale green-dashed box) and flood (pale blue-dashed horizontal striped box) material for (a) terrestrial (C_{27} , C_{29} , C_{31} , and C_{33}), (b) algal (C_{15} , C_{17} , and C_{19}), and (c) macrophyte (C_{21} and C_{23}) *n*-alkanes. Within each box, the line is the median, the X is the mean, and points outside of the box are outliers.

macrophyte *n*-alkanes (C_{21} and C_{23}) and algal *n*-alkanes (C_{15} , C_{17} , and C_{19}) compared to background sediment, although concentrations were highly variable within each classification ($p = 0.11$ and $p = 0.10$) (Figures 4 and 5). Higher concentrations of representative biomarker *n*-alkanes (i.e., terrestrial, macrophyte, and the algal *n*-alkanes) strongly correlate with the lower $\delta^{15}\text{N}$ isotopic signatures measured in flood sediments (Figure 4). Flood events are also characterized by higher CPI ratios relative to background sediment, but this difference is not significant due to the high variability in the measurements ($p = 0.13$).

Turbidite terrestrial and algal *n*-alkane compositions are most similar to background sediment (Table 3 and Figure 5). Turbidites also have a macrophyte concentration indistinguishable from either background or flood sediment ($p = 0.17$). Drought sediments are characterized by the lowest CPI and terrestrial *n*-alkane concentration of all of the sediments measured (Table 3 and Figure 5). Terrestrial *n*-alkanes comprise just 58% of the total *n*-alkane composition in droughts, while algal *n*-alkanes are the highest of all of the sediment types measured, 28% of the total *n*-alkane signal (Figure 6).

Sediment trap samples are dominated by terrestrial *n*-alkanes followed by a large contribution of algal *n*-alkanes (Table 3 and Figures 5 and 6). Macrophyte *n*-alkane concentrations, however, are low for both flood and background sediment traps; flood sediment macrophytes are below detection. Overall, sediment

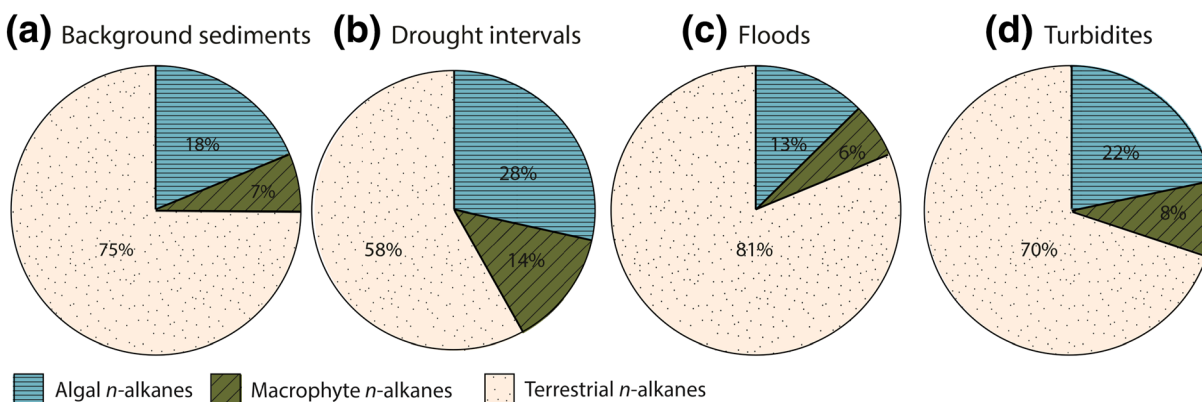


Figure 6. The relative contribution of *n*-alkane sources in Santa Barbara Basin sediments: (a) background sediments, (b) drought intervals, (c) flood events, and (d) turbidites. Terrestrial *n*-alkanes (C_{27} , C_{29} , C_{31} , and C_{33} ; tan, speckled shading) dominate all sediment types. Macrophyte *n*-alkanes (C_{21} and C_{23}) are depicted by the dark green shading with diagonal lines, and algal *n*-alkanes (C_{15} , C_{17} , and C_{19}) are depicted by the blue shading with horizontal lines.

traps have higher abundances of algal *n*-alkanes compared to the sediment core background ($p = 0.05$). The sediment trap flood CPI is indistinguishable from the flood sediment; however, the sediment trap background CPI is more than double that of the sediment background. We attribute this difference to the reduced elapsed time available for degradation in the sediment trap (weeks vs. years).

3.3. TOC Burial

The average sedimentation rate for SBB background sediment is 0.95 ± 0.19 mm year⁻¹ and the TOC burial rate is 0.43 ± 0.09 g cm⁻² kyr⁻¹ (Table 4). The sedimentation rate significantly increases in both flood ($p = 0.01$) and turbidite layers ($p = 0.01$), which are assumed to be geologically instantaneous. The sediment accumulation rate for flood sediment is 38.30 ± 34 mm year⁻¹ and has a TOC burial rate of 11.52 ± 8.90 g cm⁻² kyr⁻¹. The sedimentation rate for turbidities is 61.74 ± 32 mm year⁻¹, with an OC burial rate of 24.37 ± 12.40 g cm⁻² kyr⁻¹. Conversely, the sedimentation rate and mass accumulation rate for drought sediment are nearly half that of background sediment ($p = 0.01$).

Due to the prolonged and relatively low sedimentation rates, background and drought sediments are combined into a “non-event” sedimentation category. Non-event sedimentation is responsible for 75% of the TOC buried over the past 2,000 years (Figure 7). Of the different classes of *n*-alkanes measured, non-event sedimentation is responsible for 72% of total algal OC buried, 58% of macrophyte OC buried, and 59% of terrestrial OC buried. Flood events account for 11 of the past 2,000 years (less than 1% of time and assuming instantaneous burial) and are responsible for 8% of the TOC buried. Floods contribute 14% of the total algal OC buried, 28% of the total macrophyte OC buried, and 31% of the total terrestrial OC buried over the past 2,000 years. Turbidites account for 6 of the 2,000 years studied (less than 1% of time) and are responsible for remobilizing 13% of the TOC buried over the past 2,000 years and buried 14% of the total algal OC, 15% of the total macrophyte OC, and 10% of the total terrestrial OC in the deep basin. It is important to note that the above estimates assume that *n*-alkanes are representative of the bulk OC deposited and buried from a specific source (see section 4.4).

Table 4
Sedimentation and Burial Rates in Santa Barbara Basin Sediments

	Sedimentation rate (mm year ⁻¹)	Mass accumulation rate (g cm ⁻² year ⁻¹)	OC burial rate (g cm ⁻² kyr ⁻¹)	Terrestrial burial rate (μg cm ⁻² kyr ⁻¹)	Macrophyte burial rate (μg cm ⁻² kyr ⁻¹)	Algal burial rate (μg cm ⁻² kyr ⁻¹)
Background ($n = 7$)	0.95 ± 0.19	0.0236 ± 0.04	0.43 ± 0.09	9.61 ± 6.27	0.84 ± 1.22	2.43 ± 0.10
Drought ($n = 5$)	0.85 ± 0.14	0.0107 ± 0.002	0.42 ± 0.07	6.41 ± 3.27	1.35 ± 1.93	2.99 ± 2.54
Flood ($n = 12$)	38.30 ± 34^a	0.6205 ± 0.51	11.52 ± 8.9	439 ± 612	37.3 ± 74.4	67.6 ± 112
Turbidite ($n = 6$)	61.74 ± 32^a	0.8359 ± 0.45	24.37 ± 12.4	578 ± 548	72.2 ± 111.8	188 ± 155

^a Assuming each event has a duration of 1 year.

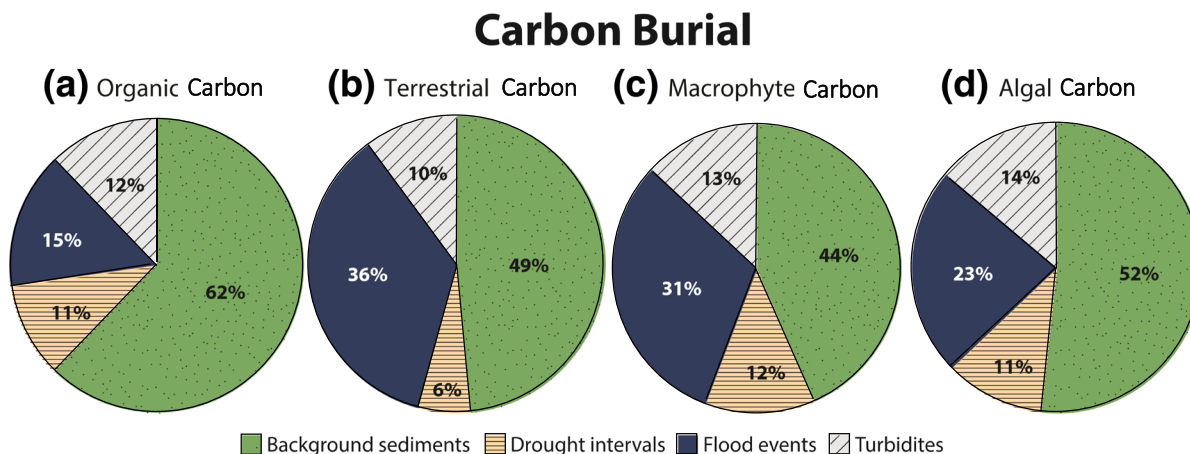


Figure 7. The relative contribution of each sediment type to burial of total organic carbon and different *n*-alkane sources in SBB sediments. Carbon burial is divided into: (a) organic carbon, (b) terrestrial (C_{27} , C_{29} , C_{31} , and C_{33}) carbon, (c) macrophyte (C_{21} and C_{23}) carbon, and (d) algal (C_{15} , C_{17} , and C_{19}) carbon, where green speckled shading represents background sediments, tan horizontally striped shading represents drought intervals, dark blue shading represents flood events sediments, and gray diagonal shading represents turbidites.

4. Discussion

4.1. Terrestrial-Sourced OM Dominates Flood Sediment

All flood sediments were dominated by terrestrially sourced OM. Sediments from flood periods contained significantly lower TOC and had the most depleted $\delta^{13}C$ ($-24.34 \pm 0.84\text{‰}$) and $\delta^{15}N$ ($6.26 \pm 0.84\text{‰}$) values (Figures 2 and 3), consistent with nonmarine sources of OM (Meyers, 1994; Sweeney & Kaplan, 1980). The $\delta^{15}N$ signature of flood sediments is significantly lower than background, turbidite, and drought sediments, with fluctuations of $>1.5\text{‰}$ that are substantially greater than the $\pm 0.5\text{‰}$ (Figure 3e) associated with changes in water column mixing, biological utilization, and oxygen availability (e.g., Wang, Hendy, & Thunell, 2019; see section 1.2). These flood sediments, however, are not as depleted as the $\sim 2\text{‰}$ reported by Sweeney and Kaplan (1980) in terrestrial sewage effluent, suggesting a mixed marine and terrestrial sediment source. In addition, *n*-alkane concentrations from terrestrial sources (e.g., long-chain length *n*-alkanes C_{27} , C_{29} , and C_{31}) are almost 3 times higher than that measured in background sediments and are 81% of the total *n*-alkanes measured (Table 3 and Figures 5 and 6). These results are consistent with previous work showing that long-chain *n*-alkanes dominate the *n*-alkane composition of SBB sinking particles and sediments (Bray & Evans, 1961; Crisp et al., 1979). Finally, terrestrial OM sources in flood sediments are also in agreement with lithogenic element concentrations that indicate terrestrial origins (Hendy et al., 2015). Combined, these results support our conclusions that a substantial component of flood sediments is derived from terrestrial OM.

The most likely source of the terrestrially derived OM in flood sediments is the numerous rivers that drain into the SBB. The Santa Clara River is considered to be the dominant contributor of basin sediment since it has the highest riverine discharge and generally carries the largest sediment load (Warrick et al., 2005). The Santa Clara and Santa Ynez Rivers have low $\delta^{13}C$ values characteristic of terrestrial OC ($\delta^{13}C < -31.5\text{‰}$, Table 2). However, the $\delta^{15}N$ of flood event sediments is most similar to the $\delta^{15}N$ of the Santa Ynez and Ventura River sediments ($\delta^{15}N < 6.3\text{‰}$). These $\delta^{15}N$ isotopic values are consistent with inorganic analyses of river sediments that indicate that the 1861–1862 and 1761 A.D. flood events contain lithogenic sediment derived from the southern slopes of the Santa Ynez and Topatopa Mountains that lie in the Santa Ynez and Ventura River catchments (Napier et al., 2019). Therefore, based on the combined $\delta^{13}C$ and $\delta^{15}N$ results, the Santa Ynez and Ventura Rivers potentially contribute more terrestrial sediment to SBB during floods than during intervals of background sedimentation.

Terrestrial material is likely transported into the SBB via two different pathways. During winter rainfall and flood events, sediment is dispersed in both surface waters and subsurface hyperpycnal plumes that are transported to the center of the SBB (Thornton, 1984, 1986; Thunell, 1998; Warrick et al., 2007; Warrick &

Farnsworth, 2009). These subsurface hyperpycnal flows of denser material may bypass the sediment traps deployed shallower in the water column and may explain differences between flood sediments and sediment trap material (Mulder & Syvitski, 1995). Another mechanism is associated with spring blooms (Thunell et al., 1995). Terrestrial (also termed lithogenic) particles typically have smaller grain sizes that sink slower. During the spring, these small particles scavenge onto larger biogenic particles and thus sink rapidly to the seafloor (Ransom et al., 1998; Thunell, 1998). This hypothesis is supported by data presented by Davis et al. (2019), who measured a lower $\delta^{15}\text{N}$ signal associated with terrestrially derived OM in deep sediment trap material (500 m) during the spring bloom.

During deposition of flood layers, extremely high precipitation rates lead to increased river discharge and deliver more terrestrial material to the continental margin over short time intervals, increasing sedimentation rates (Figure 7 and Table 4) (Ropelewski & Halpert, 1989; Warrick & Farnsworth, 2009). These higher sedimentation rates are also characterized by lower TOC and TN concentrations due to dilution of less OM-rich terrestrial material (Table 1). The average sedimentation rate across the entire SBB record is $\sim 1 \text{ mm year}^{-1}$ (mass accumulation rate = $0.0236 \pm 0.04 \text{ g cm}^{-2} \text{ year}^{-1}$) (Emery & Hülsemann, 1962; Emmer & Thunell, 2000; Thunell, 1998) with the sedimentation rate decreasing during drought intervals (Du et al., 2018). Assuming each flood layer is deposited as a single event spanning a year, the average sedimentation (and mass accumulation) rates increase during floods by a factor of 30 (e.g., Table 4, Figure 7) (Emery & Hülsemann, 1962; Emmer & Thunell, 2000; Thunell, 1998). Some flood layers (e.g., 53 A.D.) are considerably thicker than others (Figure 3), resulting in sediment and mass accumulation rates 2 orders of magnitude higher than most flood events. These rates should be considered maxima, as flood events may occur over several years or more, potentially resulting in lower accumulation rates. Despite the lower TOC concentrations, flood events are still responsible for burying OC at a rate >25 times faster than that of background and drought periods. Therefore, flood events have the capacity to rapidly bury large amounts of terrestrial OC and likely play an important role in carbon sequestration on continental margins.

4.2. Turbidites

Turbidites appear to be a mixture of terrestrial and marine biogenic material. In addition to having significantly lower average $\delta^{13}\text{C}$ signatures ($-22.57 \pm 0.25\text{‰}$) relative to background and drought sediments ($p < 0.001$), they also have lower TOC and TN concentrations, consistent with dilution by terrestrial material as evidenced by Hendy et al. (2015). The $\delta^{15}\text{N}$ signatures and terrestrial *n*-alkane concentrations of turbidites, however, are not significantly different from those measured in background sediments (Tables 1 and 3 and Figures 2 and 5). We hypothesize that turbidites remobilize oxygenated shelf sediments with a larger concentration of terrestrial material and transport it into the deep basin. Once in the deep basin, Schimmelmann et al. (2013) found that surface sediment may be resuspended prior to the turbidity current settling on the seafloor. While the resuspension and mixing of material may contribute to the similarity in $\delta^{15}\text{N}$ between turbidites and background sediment, we hypothesize that this is unlikely since the age model surrounding the turbidite deposits was not disrupted (Hendy et al., 2013).

Turbidites result in an instantaneous sedimentation rate of $61.74 \pm 32 \text{ mm year}^{-1}$ (Table 4). This is comparable to previously measured turbidite sedimentation rates in the SBB (Soutar et al., 1977). Turbidite mass accumulation rates are the highest of all the sediment types measured, reaching $0.84 \text{ g cm}^{-2} \text{ year}^{-1}$, 30% higher than that measured in flood sediments and 40 times higher than that measured in background and drought sediments (Figure 7). The rates of TOC burial in turbidites are double the rates measured in flood events and more than 50 times higher than those measured in background and drought sediments due to the higher TOC concentrations measured in turbidite sediments.

4.3. All Sediments Contain Marine-Sourced OM

Although terrestrial material is important in both flood and turbidite samples, all of the sediment types analyzed in this study contain marine-derived OM. The magnitude of this marine contribution, however, varies across sediment types and is most evident in the $\delta^{13}\text{C}$ and $\delta^{15}\text{N}$ sediment signatures, and the relative marine algal and macrophyte *n*-alkane abundances. Background and drought sediments have $\delta^{13}\text{C}$ signatures of $\sim -22\text{‰}$, consistent with marine phytoplankton versus vascular land plants (Meyers, 1994; Sweeney & Kaplan, 1980). The $\delta^{15}\text{N}$ signatures of background, turbidite, and drought sediments are also

consistent with the $\sim 7.5\text{‰}$ measured in open ocean marine OM (Sweeney & Kaplan, 1980) and the $\sim 7.88\text{‰}$ measured by Emmer and Thunell (2000) in SBB sediments over the past 15,000 years.

Variability within $\delta^{15}\text{N}$ sediment signatures may point to larger-scale changes in SBB hydrography. Smaller variations in $\delta^{15}\text{N}$ signatures of $<1.5\text{‰}$ between turbidite layers (Figure 3) are likely due to differences in the relative magnitude of terrestrial OM remobilization during each event. In contrast, variations in background and drought $\delta^{15}\text{N}$ signatures are likely due to larger-scale oscillations in water column mixing, biological utilization, and oxygen availability (Emmer & Thunell, 2000; Hendy et al., 2004; Tems et al., 2015; Wang, Hendy, & Thunell, 2019) as terrestrial inputs during drought periods should be minimized with decreased freshwater flow (as also supported by *n*-alkane composition; see Figure 6). Previous work shows a strong coherence between $\delta^{15}\text{N}$, TOC, and drought in the SBB during the past 2,000 years (Wang, Hendy, & Thunell, 2019). They attribute this strong relationship to an increase in SBB upwelling intensity that is hypothesized to occur in response to the position and strength of the North Pacific High atmospheric pressure system. This change in atmospheric circulation suppresses rainfall and creates persistent northerly winds that drive upwelling and OM export on the California Margin (Checkley & Barth, 2009). Enhanced equatorial upwelling associated with stronger trade winds may also lead to expansion of the oxygen minimum zone (OMZ) in the Eastern Tropical North Pacific due to increased OM remineralization (Deutsch et al., 2014). As the OMZ expands, the $\delta^{15}\text{N}$ of nitrate also increases, and this signal could potentially be advected from the Eastern Tropical North Pacific into the SBB by the California Undercurrent.

The *n*-alkane composition of each sedimentation type provides an additional indicator of both marine and macrophyte algae inputs to deep basin sediments. Short-chain *n*-alkanes are typically derived from non-vascular plant sources and, here, represent marine-derived algal material. Macrophyte *n*-alkanes, or midchain-length *n*-alkanes, are most likely derived from giant kelp, *M. pyrifera*, which is abundant along the SBB shoreline (Schimmelmann & Tegner, 1991). Background sediments had the lowest concentrations of algal and macrophyte *n*-alkanes compared with flood and turbidite sediments. Drought sediments have similar marine algal and macrophyte *n*-alkane concentrations, but higher relative percentages of these constituents due to the lower abundance of terrestrial *n*-alkanes, consistent with reduced river runoff-derived sediment during low rainfall years (Figure 6). Combined, marine sources of *n*-alkanes account for $<42\%$ of the total *n*-alkanes measured, and the variability in the relative percentage of this marine component is mainly due to the fluctuating amount of terrestrial-derived *n*-alkanes in the different types of sediments.

While flood sediments are dominated by terrestrial signatures (see section 4.1), algal and macrophyte *n*-alkane concentrations, although variable, remain the highest in flood sediments, with a ~ 2 -fold to 3-fold increase relative to the other sediments (Table 3). During floods, the higher algal signal is likely the result of increased riverine discharge carrying more nutrients into the SBB or storm-related mixing bringing more nutrients from depth into the photic zone, as both stimulate phytoplankton growth (Ogston & Sternberg, 1999; Otero & Siegel, 2004; Waliser & Guan, 2017; Warrick et al., 2005; Wroblewski & Richman, 1987). Previous work by Warrick et al. (2005) in the SBB found that episodic rain events increase nutrient discharge into the basin. Furthermore, they found that algal biomass was highest in the surface waters of the central basin rather than in the mouth of the Santa Clara River, which would suggest that the algal signal is predominantly derived from marine algae rather than freshwater. A marine algal signal is further confirmed by the river end members, which did not show any algal material present, although they were not collected during a flood event.

Flood and, to a lesser extent, turbidite sediments contain marine macrophyte *n*-alkane (midchain length, C_{21} and C_{23}) concentrations that are higher than those measured in drought and background sediments ($p = 0.10$; $p = 0.17$). In flood sediments, marine macrophyte contributions are variable, ranging from about double those measured in the other sediment types (Table 3 and Figure 5) to below detection. Kelp can die due to age, grazing, or destruction by waves prior to being deposited on the ocean floor (Cavanaugh et al., 2011). Severe storms and floods have been observed to cause widespread destruction of kelp forests, substantially reducing their biomass (Schimmelmann & Tegner, 1991). Based on our data, we hypothesize that flood-producing storms can be associated with kelp forest destruction with their remains transported into the deep basin where the OC is incorporated into the sediments. Since not all flood events contained macrophyte *n*-alkanes, we hypothesize that some storm-induced transport is weaker, minimizing kelp die-off. This hypothesis is supported by low macrophyte concentrations, which also correlate strongly

with low algal concentrations in flood sediments ($R^2 = 0.77$, data not shown), suggesting weaker ocean mixing or river discharge during those events. Therefore, even though the kelp itself does not originate from land, the processes that transport large quantities of material off shore (e.g., floods and turbidites) also carry significant quantities of kelp-derived material.

4.4. Utility of *n*-Alkanes Proxy for Sediment Source

Lipid biomarkers, specifically *n*-alkanes, were chosen as a potential proxy for sediment source due to their known resistance to degradation compared to other forms of OM containing nitrogen and phosphorus (Eglinton et al., 1991; Meyers & Ishiwatari, 1993). Of the lipid biomarkers typically used (e.g., *n*-alkanes, ketones, alcohols, and fatty acids), the *n*-alkane class is the least reactive and slowest to degrade (Wakeham et al., 1997). Constraining *n*-alkane degradation by chain length has been challenging due to the variety of factors that influence degradation in the water column and sediments, including redox, salinity, temperature, pressure, sediment matrix, and microbial community composition (Canuel & Martens, 1996; Lamontagne et al., 2004; Lofthus et al., 2018; Schwarz et al., 1974; Wang, Yang, et al., 2019). For example, during transport and arrival at the seafloor, *n*-alkanes have been shown to be a potential energy source under both aerobic and anaerobic conditions (Caldwell et al., 1998; Young & Phelps, 2005). Lacustrine sediment trap studies over the upper 100 m of the water column have found that degradation rate varies by chain length depending on sediment matrix and community composition in bottom waters (Meyers et al., 1984; Meyers & Eadie, 1993).

In sediments, Canuel and Martens (1996) found that the greatest rate of degradation occurred in midchain-length *n*-alkanes (C_{23} – C_{27}), while short- (C_{17} – C_{21}) and long-chain *n*-alkanes ($>C_{25}$) had slower degradation rates. In contrast, Lofthus et al. (2018) found that short-chain *n*-alkanes (C_{13} – C_{15}) had the highest degradation rates and that long-chain *n*-alkane degradation (C_{26} – C_{36}) rates varied in water temperatures between 5°C and 10°C. Indeed, many studies of microbial-facilitated *n*-alkane degradation have shown substrate preferences for either short- or long-chain *n*-alkanes depending on the species present in the sediment (Bihari et al., 2010; Liu et al., 2014; So & Young, 1999; Whyte et al., 1998).

Due to the uncertainty in *n*-alkane degradation by chain length and the lack of a site-specific study, we used other proxies to consider potential degradation impacts on our results. First, we examined the CPI with increasing depth (time) in the core. A lower CPI is typically indicative of greater degradation. No trend in the CPI with increasing core depth is observed ($R^2 < 0.001$), as the source of fresh OM input dominates the *n*-alkane signal (supporting information Figure S1). We further found only trace amounts of phytane and pristane, degradation products of chlorophyll, and there were no trends in their concentrations with depth. Therefore, *n*-alkane degradation with increasing depth in the core is assumed to be minimal.

The relative distributions of *n*-alkanes may be further altered by secondary processes, such as production of odd chain *n*-alkanes by microbes in sediments. Li et al. (2018) specifically measured anaerobic microbe production of alkanes in peat and found that microbes produced a negligible amount of long-chain and mid-chain *n*-alkanes. However, these anaerobic microbes did produce the short-chain alkane, C_{19} , at a rate of 0.5% per year. Here, C_{19} production by microbes was assumed to be negligible since very few of our samples contained C_{19} . Samples that did contain C_{19} showed no trend in concentration with depth ($R^2 = 0.04$; Figure S2). Thus, there is no evidence that secondary processing by microbial activity influences our results.

One final issue to consider is the limitation of source attribution of *n*-alkanes based on chain length alone. Historically, long-chain *n*-alkanes have been primarily attributed to terrestrial material. However, terrestrial sources may also produce a small amount of short-chain *n*-alkanes (Kuhn et al., 2010). Similarly, algal sources have been found to produce some long-chain alkanes (Lichtfouse et al., 1994). As such, samples with mixed *n*-alkane signatures may underestimate or overestimate a specific source. Other measurements in this study (e.g., trace elements, $\delta^{13}C$, and $\delta^{15}N$), however, confirm similarly high proportions of terrestrially derived material. Stable isotope ($\delta^{13}C$ and $\delta^{15}N$) signatures during flood events are 2‰ and 4‰ lower, respectively, than background, turbidite, and drought sediments and are consistent with terrestrial OM values (Meyers, 1994; Sweeney & Kaplan, 1980). Additionally, SXRF data show significantly higher concentrations of lithogenic elements (Hendy et al., 2015). Combined, these results confirm the utility of the *n*-alkanes in characterizing source material in these sediments.

4.5. Flood and Turbidite Sediment Contributions to OC Burial

In order to link modern processes with those observed in the sedimentary record, we examined sediment trap material associated with 1997–1998 El Niño flooding. The 1997–1998 El Niño was one of the wettest years on record with 202 mm of rainfall and an eightfold increase in lithogenic sedimentation rates in SBB (Lange et al., 2000; Ross et al., 1998; Thunell, 2003). The 1997–1998 El Niño sediment trap material is characterized by lower isotopic values and higher terrestrial *n*-alkane concentrations relative to the background sediment trap, consistent with the increase in terrestrial OM deposition. However, the El Niño sediment trap material contained no macrophyte material, despite observations of kelp bed destruction during that time (Lange et al., 2000). Compared to the sediment core, the sediment traps have lower C/N ratios, consistent with fresher sediment input, and isotopic ($\delta^{13}\text{C}$ and $\delta^{15}\text{N}$) signatures similar to background core sediments. Furthermore, flood sediment trap terrestrial *n*-alkane concentrations are significantly lower than those measured in the sediment core paleoflood events.

We hypothesize two mechanisms to explain the compositional differences between the 1997–1998 El Niño sediment trap and flood layer sediments. First, the kelp rafts and flood plumes bypassed the sediment trap; kelp rafts may have been too large to pass through the sediment trap honeycomb, and flood plumes may have been transported downslope via gravity rather than settling from the surface waters (see section 4.2). Second, the processes that contribute to the flood layers in SBB are significantly different than those associated with flooding during the 1997–1998 El Niño.

Previous studies of SBB sediments have hypothesized the occurrence of megafloods; (Du et al., 2018; Schimmelmann et al., 1998; Schimmelmann et al., 2003); extreme floods are associated with atmospheric rivers that produce massive amounts of precipitation and storm conditions (Dettinger et al., 2011; Neiman et al., 2008). The most recent megaflood to occur in California was in 1861–1862 and is documented in the sediment core. The 1861–1862 megaflood, or “The Great Flood,” occurred after ~40 days of continuous rain and historical reports of 25 in. that winter (Dettinger & Ingram, 2013; Newbold, 1991). Megaflood layers in the sediment core occur every 166 ± 48 years in SBB, arguing that such events bury significant quantities of OC over a short time period. These 11 flood events are responsible for 15% of the TOC buried over the last 2,000 years. The largest flood event in the record (53 A.D.) may have accounted for 3% of the TOC buried alone. Furthermore, flood events are much more efficient in burying macrophyte- and terrestrial-derived OC, components that may have otherwise been remineralized in shallower oxygenated sediments if not transported and buried in the deeper ocean.

The six turbidites measured are responsible for remobilizing 12% of the TOC buried in the deep basin over the past 2,000 years. Although turbidites also play a large role in C burial through high burial rates, this C was likely remobilized from the shelf. Turbidites therefore do not contribute to new C burial but rather redistribute OC into low-oxygen deep waters of the SBB where remineralization is likely to be slower (Burdige, 2006). Non-event (background + drought) sediments are responsible for the bulk (75%) of the TOC buried, though at a much slower rate compared to flood or turbidite sediments. Regardless of the sedimentation process, the SBB buries a significant amount of OC from terrestrial and marine algal sources (Figure 7).

4.6. The Role of Terrestrial OM and Episodic Events in the Carbon Cycle

The burial of OC in oceanic sediments is a major sequestration pathway for carbon dioxide on geologic time-scales with continental shelves representing the largest sink of both terrestrially and marine-derived OC in the global ocean (Bernier, 1982; Hedges & Keil, 1995; Martin et al., 1987; Sarmiento & Sundquist, 1992). Indeed, estimates suggest that deltas and shelf sediments bury 30–35% of all of the terrestrially derived OC delivered by rivers globally (Kandasamy & Nath, 2016). However, understanding OC sources, mechanisms of delivery, and burial along continental margins is complicated by their spatial and temporal complexity, making predictions of the long-term controls on the net drawdown of atmospheric carbon dioxide over past, modern-day, and future regimes difficult to assess (e.g., Bianchi et al., 2018). One such hot spot of OC burial along the coast is small mountain river systems, such as those that deposit into the SBB, which may deliver as much as half of the world’s global particulate OM to continental shelf systems (Bao et al., 2015; Hatten et al., 2010; Hedges & Keil, 1995). This delivery may be highly episodic in nature as high relief and exposure to intense storm events result in turbid flow. Studies of continental margins have increasingly

found that terrestrial OM is a much greater component of marine burial than previously realized (e.g., Blair et al., 2004; Burdige, 2005; Bianchi, 2011). For example, in the Northern Gulf of Mexico, terrestrial OM accounted for 70–80% of OM burial (Gordon & Goñi, 2003), and off the coast of Washington, terrestrial OM comprised 10–30% of the sediment on the continental margin (Keil et al., 1994; Prahl et al., 1994).

Our study confirms these results; SBB sediments are composed of substantial terrestrial OC. Although relatively infrequent, 11 flood events, comprising less than 1% of the total 2,000 year record analyzed in this study, contribute 31% of all terrestrially derived OC buried. Terrestrial OM burial in marine sediments is an important climate feedback mechanism as the OC is often derived from vegetation and soil versus bedrock. Higher burial efficiencies relative to that on land coupled with this fresher nonrock-derived OC result in marine terrestrial OM burial being an important sink of atmospheric CO₂ (Stallard, 1998). Episodic floods occur worldwide (e.g., Hilton et al., 2008) and are likely to increase due to climate change (EASAC, 2018). Western Europe in particular is susceptible to atmospheric river-induced floods (Lavers & Villarini, 2015), and areas surrounding the Pacific Ocean are susceptible to ENSO-related flooding (Muis et al., 2018). Our results highlight the complexity of the C cycle at the land-ocean interface and how episodic climate events may disproportionately impact C biogeochemistry. Incorporating these regions and episodic drivers of terrestrial OC burial into larger-scale C cycle models is therefore critical for understanding past, present, and future C dynamics in light of increased flooding, sea-level rise, and changes in land use.

5. Conclusions

Terrestrial OM is the dominant source of C buried in the SBB across all forms of deposition: flooding, turbidite remobilization, drought, and background conditions. Non-event sedimentation in the SBB is responsible for 75% of the TOC buried over the last 2,000 years. Burial rates under these conditions are low ($\sim 0.43 \text{ g cm}^{-2} \text{ kyr}^{-1}$), and OM sources include significant marine algal and macrophyte contributions. Droughts had a minimal impact on OC burial; however, they are composed of a larger proportion of marine material compared to the baseline. Episodic events (turbidites and floods) account for 25% of the OC buried, which is significant as these events occur over less than 1% of the time studied. While turbidites do not sequester new OC in SBB sediments, these events are responsible for the rapid remobilization of OC from the shelf to the deep basin. Turbidites contribute $\sim 13\%$ of the TOC buried in deep sea sediments over the past 2,000 years, with buried OC containing the highest concentrations of marine algal and macrophyte C relative to background, drought, and flood sedimentation.

Floods have the potential to bury significant amounts of OC in marine sediments through geologic time. In SBB, floods on the scale of megafloods are rare, occurring every 166 ± 48 years in the SBB, but have buried 11% of the TOC throughout the past 2,000 years. The main source of OC buried during these episodic flood events is terrestrially derived and is less degraded than terrestrial OC buried during background sedimentation. However, algae and macrophytes are still significant contributors to flood sediments. Increased algal concentrations in flood sediments are likely due to increased nutrient loads from river runoff and storm-driven mixing. Additionally, macrophyte deposition in flood sediments is likely associated with the destruction of kelp forests by waves during flood-associated storms. These results may be more widely relevant as episodic floods and turbidites, as well as drought intervals, are not limited to the Southern California region. Our results confirm that these processes may play a critical role in OC burial on continental margins around the world.

Data Availability Statement

Data will be provided as supporting information and will be available online (<https://doi.org/10.1594/PANGAEA.917989>).

References

- Altabet, M. A., Pilskaln, C., Thunell, R., Pride, C., Sigman, D., Chavez, F., & Francois, R. (2020). The nitrogen isotope biogeochemistry of sinking particles from the margin of the Eastern North Pacific. *Deep Sea Research Part I: Oceanographic Research; Papers*, 46(4), 655–679. [https://doi.org/10.1016/s0967-0637\(98\)00084-3](https://doi.org/10.1016/s0967-0637(98)00084-3)
- Bao, H., Lee, T., Huang, J., Feng, X., Dai, M., & Kao, S. (2015). Importance of Oceanian small mountainous rivers (SMRs) in global land-to-ocean output of lignin and modern biospheric carbon. *Scientific Reports*, 5(1), 16217. <https://doi.org/10.1038/srep16217>

Acknowledgments

We would like to thank My (Phoebe) Le for her assistance in processing the samples. C. R. B.-N., C. V. D., C. T. S., and R. C. T. were supported by the National Science Foundation (NSF) OCE Grant 1631977. I. L. H. was supported the NSF OCE Grant 1304327. We thank Dorothy Pak for her assistance in the collection of kelp samples, Tiffany Napier for river bed load samples, and Yi Wang for sampling SPR0901-03KC.

- Barron, J. A., Bukry, D., & Field, D. (2010). Santa Barbara Basin diatom and silicoflagellate response to global climate anomalies during the past 2200 years. *Quaternary International*, 215(1–2), 34–44. <https://doi.org/10.1016/j.quaint.2008.08.007>
- Barron, J. A., Bukry, D., & Hendy, I. L. (2015). High-resolution paleoclimatology of the Santa Barbara Basin during the Medieval Climate Anomaly and early Little Ice Age based on diatom and silicoflagellate assemblages in Kasten core SPR0901-02KC. *Quaternary International*, 387, 13–22. <https://doi.org/10.1016/j.quaint.2014.04.020>
- Berner, R. A. (1982). Burial of organic carbon and pyrite sulfur in the modern ocean; its geochemical and environmental significance. *American Journal of Science*, 282(4), 451–473. <https://doi.org/10.2475/ajs.282.4.451>
- Bianchi, T. S. (2011). The role of terrestrially derived organic carbon in the coastal ocean: A changing paradigm and the priming effect. *Proceedings of the National Academy of Sciences*, 108(49), 19473–19481. <https://doi.org/10.1073/pnas.1017982108>
- Bianchi, T. S., Cui, X., Blair, N. E., Burdige, D. J., Eglinton, T. I., & Galy, V. (2018). Centers of organic carbon burial and oxidation at the land-ocean interface. *Organic Geochemistry*, 115, 138–155. <https://doi.org/10.1016/j.orggeochem.2017.09.008>
- Bihari, Z., Szabó, Z., Szvetnik, A., Balázs, M., Bartos, P., Tolmacsov, P., et al. (2010). Characterization of a novel long-chain *n*-alkane-degrading strain, *Dietzia* sp. E1. *Zeitschrift Für Naturforschung C*, 65(11–12), 693–700. <https://doi.org/10.1515/znc-2010-11-1210>
- Blaauw, M., & Christen, J. A. (2011). Flexible paleoclimate age-depth models using an autoregressive gamma process. *Bayesian Analysis*, 6(3), 457–474. <https://doi.org/10.1214/11-BA618> <https://projecteuclid.org/euclid.ba/1339616472>
- Blair, N. E., Leithold, E. L., & Aller, R. C. (2004). From bedrock to burial: The evolution of particulate organic carbon across coupled watershed-continental margin systems. *Marine Chemistry*, 92(1–4), 141–156. <https://doi.org/10.1016/j.marchem.2004.06.023>
- Blumer, M., & Clark, R. C. Jr. (1967). Distribution of *n*-paraffins in marine organisms and sediment. *Limnology and Oceanography*, 12(1), 79–87. <https://doi.org/10.4319/lo.1967.12.1.0079>
- Bograd, S. J., & Lynn, R. J. (2001). Physical-biological coupling in the California Current during the 1997–99 El Niño-La Niña Cycle. *Geophysical Research Letters*, 28(2), 275–278. <https://doi.org/10.1029/2000gl012047>
- Bograd, S. J., Schwing, F. B., Castro, C. G., & Timothy, D. A. (2002). Bottom water renewal in the Santa Barbara Basin. *Journal of Geophysical Research*, 107(C12). <https://doi.org/10.1029/2001jc001291>
- Brandes, J. A., Devol Allan, H., Yoshinari, T., Jayakumar, D. A., & Naqvi, S. W. A. (2003). Isotopic composition of nitrate in the central Arabian Sea and eastern tropical North Pacific: A tracer for mixing and nitrogen cycles. *Limnology and Oceanography*, 43(7), 1680–1689. <https://doi.org/10.4319/lo.1998.43.7.1680>
- Bray, E., & Evans, E. (1961). Distribution of *n*-paraffins as a clue to recognition of source beds. *Geochimica et Cosmochimica Acta*, 22(1), 2–15. [https://doi.org/10.1016/0016-7037\(61\)90069-2](https://doi.org/10.1016/0016-7037(61)90069-2)
- Bray, N. A., Keyes, A., & Morawitz, W. M. (1999). The California Current system in the Southern California Bight and the Santa Barbara Channel. *Journal of Geophysical Research*, 104(C4), 7695–7714. <https://doi.org/10.1029/1998jc900038>
- Burdige, D. J. (2005). Burial of terrestrial organic matter in marine sediments: A re-assessment. *Global Biogeochemical Cycles*, 19, Gb4011. <https://doi.org/10.1029/2004gb002368>
- Burdige, D. J. (2006). *Geochemistry of marine sediments*. Princeton: Princeton University Press.
- Caldwell, M. E., Garrett, R. M., Prince, R. C., & Sufliata, J. M. (1998). Anaerobic biodegradation of long-chain *n*-alkanes under sulfate-reducing conditions. *Environmental Science & Technology*, 32(14), 2191–2195. <https://doi.org/10.1021/es9801083>
- Canuel, E. A., & Martens, C. S. (1996). Reactivity of recently deposited organic matter: Degradation of lipid compounds near the sediment-water interface. *Geochimica et Cosmochimica Acta*, 60(10), 1793–1806. [https://doi.org/10.1016/0016-7037\(96\)00045-2](https://doi.org/10.1016/0016-7037(96)00045-2)
- Cavanaugh, K., Siegel, D., Reed, D., & Dennison, P. (2011). Environmental controls of giant-kelp biomass in the Santa Barbara Channel, California. *Marine Ecology Progress Series*, 429, 1–17. <https://doi.org/10.3354/meps09141>
- Chavez, F. P. (1996). Forcing and biological impact of onset of the 1992 El Niño in central California. *Geophysical Research Letters*, 23(3), 265–268. <https://doi.org/10.1029/96GL00017>
- Checkley, D. M., & Barth, J. A. (2009). Patterns and processes in the California Current System. *Progress in Oceanography*, 83(1–4), 49–64. <https://doi.org/10.1016/j.pocean.2009.07.028>
- Cline, J., & Kaplan, I. (1975). Isotopic fractionation of dissolved nitrate during denitrification in the eastern tropical North Pacific Ocean. *Marine Chemistry*, 3(4), 271–299. [https://doi.org/10.1016/0304-4203\(75\)90009-2](https://doi.org/10.1016/0304-4203(75)90009-2)
- Crisp, P., Brenner, S., Venkatesan, M., Ruth, E., & Kaplan, I. (1979). Organic chemical characterization of sediment-trap particulates from San Nicolas, Santa Barbara, Santa Monica and San Pedro Basins, California. *Geochimica et Cosmochimica Acta*, 43(11), 1791–1801. [https://doi.org/10.1016/0016-7037\(79\)90027-9](https://doi.org/10.1016/0016-7037(79)90027-9)
- Davis, C. V., Ontiveros-Cuadras, J. F., Benitez-Nelson, C., Schmittner, A., Osborne, E., Tappa, E., & Thunell, R. C. (2019). Ongoing increase in Eastern Tropical North Pacific denitrification as interpreted through sedimentary $\delta^{15}\text{N}$ from Santa Barbara Basin. *Paleoceanography and Paleoclimatology*, 34. <https://doi.org/10.1029/2019pa003578>
- Dettinger, M. D., & Ingram, B. L. (2013). The coming megafloods. *Scientific American*, 308(1), 64–71. <https://doi.org/10.1038/scientificamerican0113-64>
- Dettinger, M. D., Ralph, F. M., Das, T., Neiman, P. J., & Cayan, D. R. (2011). Atmospheric rivers, floods and the water resources of California. *Water*, 3(2), 445–478. <https://doi.org/10.3390/w3020445>
- Deuser, W. G., Brewer, P. G., Jickells, T. D., & Commeau, R. F. (1983). Biological control of the removal of abiogenic particles from the surface ocean. *Science*, 219(4583), 388–391. <https://doi.org/10.1126/science.219.4583.388>
- Deutsch, C., Berelson, W., Thunell, R., Weber, T., Tems, C., McManus, J., et al. (2014). Centennial changes in North Pacific anoxia linked to tropical trade winds. *Science*, 345(6197), 665–668. <https://doi.org/10.1126/science.1252332>
- Dorman, C. E., & Winant, C. D. (2000). The structure and variability of the marine atmosphere around the Santa Barbara Channel. *Monthly Weather Review*, 128(2), 261. [https://doi.org/10.1175/1520-0493\(2000\)128:0.co;2](https://doi.org/10.1175/1520-0493(2000)128:0.co;2)
- Du, X., Hendy, I., & Schimmelmann, A. (2018). A 9000-year flood history for Southern California: A revised stratigraphy of varved sediments in Santa Barbara Basin. *Marine Geology*, 397, 29–42. <https://doi.org/10.1016/j.margeo.2017.11.014>
- EASAC. (2018). *Extreme weather events in Europe* (pp. 1–8). European Academies Science Advisory Council. Retrieved from https://easac.eu/fileadmin/PDF_s/reports_statements/Extreme_Weather/EASAC_Statement_Extreme_Weather_Events_March_2018_FINAL.pdf
- Eglinton, G., Logan, G., Ambler, R., Boon, J., & Perizonius, W. (1991). Molecular preservation [and discussion]. *Philosophical Transactions: Biological Sciences*, 333(1268), 315–328. <https://doi.org/10.1098/rstb.1991.0081>
- Emery, K., & Hülsemann, J. (1962). The relationships of sediments, life and water in a marine basin. *Deep Sea Research*, 8(3–4), 165–192. [https://doi.org/10.1016/0146-6313\(61\)90019-3](https://doi.org/10.1016/0146-6313(61)90019-3)
- Emmer, E., & Thunell, R. C. (2000). Nitrogen isotope variations in Santa Barbara Basin sediments: Implications for denitrification in the eastern tropical North Pacific during the last 50,000 years. *Paleoceanography*, 15(4), 377–387. <https://doi.org/10.1029/1999pa000417>

- Ficken, K., Li, B., Swain, D., & Eglinton, G. (2000). An *n*-alkane proxy for the sedimentary input of submerged/floating freshwater aquatic macrophytes. *Organic Geochemistry*, 31(7–8), 745–749. [https://doi.org/10.1016/s0146-6380\(00\)00081-4](https://doi.org/10.1016/s0146-6380(00)00081-4)
- Gordon, E. S., & Goñi, M. A. (2003). Sources and distribution of terrigenous organic matter delivered by the Atchafalaya River to sediments in the northern Gulf of Mexico. *Geochimica et Cosmochimica Acta*, 67(13), 2359–2375. [https://doi.org/10.1016/s0016-7037\(02\)01412-6](https://doi.org/10.1016/s0016-7037(02)01412-6)
- Graham, N. E., Hughes, M. K., Ammann, C. M., Cobb, K. M., Hoerling, M. P., Kennett, D. J., et al. (2007). Tropical Pacific—Mid-latitude teleconnections in medieval times. *Climatic Change*, 83(1–2), 241–285. <https://doi.org/10.1007/s10584-007-9239-2>
- Grimalt, J., Albaiges, J., Al-Saad, H. T., & Douabul, A. A. (1985). *n*-Alkane distributions in surface sediments from the Arabian Gulf. *Naturwissenschaften*, 72(1), 35–37. <https://doi.org/10.1007/bf00405327>
- Hatten, J. A., Goñi, M. A., & Wheatcroft, R. A. (2010). Chemical characteristics of particulate organic matter from a small, mountainous river system in the Oregon Coast Range, USA. *Biogeochemistry*, 107(1–3), 43–66. <https://doi.org/10.1007/s10533-010-9529-z>
- Hedges, J., Clark, W., Quay, P., Richey, J., Devol, A., & Santos, U. de M. (1986). Compositions and fluxes of particulate organic material in the Amazon River. *Limnology and Oceanography*, 31(4), 717–738. <https://doi.org/10.4319/lo.1986.31.4.0717>
- Hedges, J. I., & Keil, R. G. (1995). Sedimentary OM preservation: An assessment and speculative synthesis. *Marine Chemistry*, 49(2–3), 81–115. [https://doi.org/10.1016/0304-4203\(95\)00008-f](https://doi.org/10.1016/0304-4203(95)00008-f)
- Hendy, I. L., Dunn, L., Schimmelmann, A., & Pak, D. K. (2013). Resolving varve and radiocarbon chronology differences in the Santa Barbara basin sedimentary record, California. *Quaternary International*, 387, 136–168. <https://doi.org/10.1016/j.quaint.2015.01.142>
- Hendy, I. L., Napier, T. J., & Schimmelmann, A. (2015). From extreme rainfall to drought: 250 years of annually resolved sediment deposition in Santa Barbara Basin, California. *Quaternary International*, 387, 3–12. <https://doi.org/10.1016/j.quaint.2015.01.026>
- Hendy, I. L., Pedersen, T. F., Kennett, J. P., & Tada, R. (2004). Intermittent existence of a southern Californian upwelling cell during submillennial climate change of the last 60 kyr. *Paleoceanography*, 19(3). <https://doi.org/10.1029/2003pa000965>
- Heusser, L. E., Hendy, I. L., & Barron, J. A. (2015). Vegetation response to southern California drought during the Medieval Climate Anomaly and early Little Ice Age (AD 800–1600). *Quaternary International*, 387, 23–35. <https://doi.org/10.1016/j.quaint.2014.09.032>
- Hilton, R. G., Galy, A., Hovius, N., Chen, M.-C., Horng, M.-J., & Chen, H. (2008). Tropical-cyclone-driven erosion of the terrestrial biosphere from mountains. *Nature Geoscience*, 1(11), 759–762. <https://doi.org/10.1038/ngeo333>
- Hülsemann, J., & Emery, K. O. (1961). Stratification in recent sediments of Santa Barbara Basin as controlled by organisms and water character. *The Journal of Geology*, 69(3), 279–290. <https://doi.org/10.1086/626742>
- Kandasamy, S., & Nath, B. N. (2016). Perspectives on the terrestrial organic matter transport and burial along the land-deep sea continuum: Caveats in our understanding of biogeochemical processes and future needs. *Frontiers in Marine Science*, 3. <https://doi.org/10.3389/fmars.2016.00259>
- Keil, R. G., Montluçon, D. B., Prahl, F. G., & Hedges, J. I. (1994). Sorptive preservation of labile organic matter in marine sediments. *Nature*, 370(6490), 549–552. <https://doi.org/10.1038/370549a0>
- Kuhn, T. K., Krull, E. S., Bowater, A., Grice, K., & Gleixner, G. (2010). The occurrence of short chain *n*-alkanes with an even over odd predominance in higher plants and soils. *Organic Geochemistry*, 41(2), 88–95. <https://doi.org/10.1016/j.orggeochem.2009.08.003>
- Lamontagne, M. G., Leifer, I., Bergmann, S., Werfhorst, L. C. V. D., & Holden, P. A. (2004). Bacterial diversity in marine hydrocarbon seep sediments. *Environmental Microbiology*, 6(8), 799–808. <https://doi.org/10.1111/j.1462-2920.2004.00613.x>
- Lange, C. B., Weinheimer, A. L., Reid, F. M., Tappa, E., & Thunell, R. C. (2000). Response of siliceous microplankton from the Santa Barbara Basin to the 1997–98 El Niño event. *California Cooperative Oceanic Fisheries Reports*, 41, 186–193.
- Lavers, D. A., & Villarini, G. (2015). The contribution of atmospheric rivers to precipitation in Europe and the United States. *Journal of Hydrology*, 522, 382–390. <https://doi.org/10.1016/j.jhydrol.2014.12.010>
- Li, C., Sessions, A. L., Kinnaman, F. S., & Valentine, D. L. (2009). Hydrogen-isotopic variability in lipids from Santa Barbara Basin sediments. *Geochimica et Cosmochimica Acta*, 73(16), 4803–4823. <https://doi.org/10.1016/j.gca.2009.05.056>
- Li, G., Li, L., Tarozo, R., Longo, W. M., Wang, K. J., Dong, H., & Huang, Y. (2018). Microbial production of long-chain *n*-alkanes: Implication for interpreting sedimentary leaf wax signals. *Organic Geochemistry*, 115, 24–31. <https://doi.org/10.1016/j.orggeochem.2017.10.005>
- Lichtfouse, É., Derenne, S., Mariotti, A., & Largeau, C. (1994). Possible algal origin of long chain odd *n*-alkanes in immature sediments as revealed by distributions and carbon isotope ratios. *Organic Geochemistry*, 22(6), 1023–1027. [https://doi.org/10.1016/0146-6380\(94\)90035-3](https://doi.org/10.1016/0146-6380(94)90035-3)
- Liu, H., Xu, J., Liang, R., & Liu, J. (2014). Characterization of the medium- and long-chain *n*-alkanes degrading *Pseudomonas aeruginosa* strain SJTD-1 and its alkane hydroxylase genes. *PLoS ONE*, 9(8), e105506. <https://doi.org/10.1371/journal.pone.0105506>
- Lofthus, S., Netzer, R., Lewin, A. S., Heggeset, T. M. B., Haugen, T., & Brakstad, O. G. (2018). Biodegradation of *n*-alkanes on oil-seawater interfaces at different temperatures and microbial communities associated with the degradation. *Biodegradation*, 29(2), 141–157. <https://doi.org/10.1007/s10532-018-9819-z>
- Martin, J. H., Knauer, G. A., Karl, D. M., & Broenkow, W. W. (1987). VERTEX: Carbon cycling in the northeast Pacific. *Deep Sea Research Part B. Oceanographic Literature Review*, 34(9), 753. [https://doi.org/10.1016/0198-0254\(87\)90148-8](https://doi.org/10.1016/0198-0254(87)90148-8)
- Masiello, C. A., & Druffel, E. R. (2001). Carbon isotope geochemistry of the Santa Clara River. *Global Biogeochemical Cycles*, 15(2), 407–416. <https://doi.org/10.1029/2000GB001290>
- Meyers, P., Leenheer, M., Eadie, B., & Maule, S. (1984). Organic geochemistry of suspended and settling particulate matter in Lake Michigan. *Geochimica et Cosmochimica Acta*, 48(3), 443–452. [https://doi.org/10.1016/0016-7037\(84\)90273-4](https://doi.org/10.1016/0016-7037(84)90273-4)
- Meyers, P. A. (1994). Preservation of elemental and isotopic source identification of sedimentary OM. *Chemical Geology*, 114(3–4), 289–302. [https://doi.org/10.1016/0009-2541\(94\)90059-0](https://doi.org/10.1016/0009-2541(94)90059-0)
- Meyers, P. A. (2003). Applications of organic geochemistry to paleolimnological reconstructions: A summary of examples from the Laurentian Great Lakes. *Organic Geochemistry*, 34(2), 261–289. [https://doi.org/10.1016/s0146-6380\(02\)00168-7](https://doi.org/10.1016/s0146-6380(02)00168-7)
- Meyers, P. A., & Eadie, B. J. (1993). Sources, degradation and recycling of organic matter associated with sinking particles in Lake Michigan. *Organic Geochemistry*, 20(1), 47–56. [https://doi.org/10.1016/0146-6380\(93\)90080-u](https://doi.org/10.1016/0146-6380(93)90080-u)
- Meyers, P. A., & Ishiwatari, R. (1993). Lacustrine organic geochemistry—An overview of indicators of organic matter sources and diagenesis in lake sediments. *Organic Geochemistry*, 20(7), 867–900. [https://doi.org/10.1016/0146-6380\(93\)90100-p](https://doi.org/10.1016/0146-6380(93)90100-p)
- Muis, S., Haigh, I. D., Guimarães Nobre, G., Aerts, J. C. J. H., & Ward, P. J. (2018). Influence of El Niño-Southern Oscillation on global coastal flooding. *Earth's Future*, 6, 1311–1322. <https://doi.org/10.1029/2018EF000909>
- Mulder, T., & Syvitski, J. P. (1995). Turbidity currents generated at river mouths during exceptional discharges to the world oceans. *The Journal of Geology*, 103(3), 285–299. <https://doi.org/10.1086/629747>
- Muller-Karger, F. E., Varela, R., Thunell, R., Luerssen, R., Hu, C., & Walsh, J. J. (2005). The importance of continental margins in the global carbon cycle. *Geophysical Research Letters*, 32, L01602. <https://doi.org/10.1029/2004GL021346>

- Napier, T. J., Hendy, I. L., Fahnestock, M. F., & Bryce, J. G. (2019). Provenance of detrital sediments in Santa Barbara Basin, California, USA: Changes in source contributions between the Last Glacial Maximum and Holocene. *GSA Bulletin*, *132*(1–2), 65–84. <https://doi.org/10.1130/B32035.1>
- Neiman, P. J., Ralph, F. M., Wick, G. A., Lundquist, J. D., & Dettinger, M. D. (2008). Meteorological characteristics and overland precipitation impacts of atmospheric rivers affecting the West Coast of North America based on eight years of SSM/I satellite observations. *Journal of Hydrometeorology*, *9*(1), 22–47. <https://doi.org/10.1175/2007jhm855.1>
- Newbold, J. D. (1991). In R. W. Clottu & J. Gillespie (Eds.), *The Great California Flood of 1861–1862* (Vol. 5, pp. 1–12). Lodi, CA: San Joaquin Historical Society.
- Ogston, A., & Sternberg, R. (1999). Sediment-transport events on the northern California continental shelf. *Marine Geology*, *154*(1–4), 69–82. [https://doi.org/10.1016/S0025-3227\(98\)00104-2](https://doi.org/10.1016/S0025-3227(98)00104-2)
- Otero, M. P., & Siegel, D. A. (2004). Spatial and temporal characteristics of sediment plumes and phytoplankton blooms in the Santa Barbara Channel. *Deep Sea Research Part II: Topical Studies in Oceanography*, *51*(10–11), 1129–1149. <https://doi.org/10.1016/j.dsr2.2004.04.004>
- Pearson, A., & Eglinton, T. (2000). The origin of *n*-alkanes in Santa Monica Basin surface sediment: A model based on compound-specific $\Delta^{14}\text{C}$ and $\delta^{13}\text{C}$ data. *Organic Geochemistry*, *31*(11), 1103–1116. [https://doi.org/10.1016/S0146-6380\(00\)00121-2](https://doi.org/10.1016/S0146-6380(00)00121-2)
- Prahl, F., Ertel, J., Goni, M., Sparrow, M., & Eversmeyer, B. (1994). Terrestrial organic carbon contributions to sediments on the Washington margin. *Geochimica et Cosmochimica Acta*, *58*(14), 3035–3048. [https://doi.org/10.1016/0016-7037\(94\)90177-5](https://doi.org/10.1016/0016-7037(94)90177-5)
- Rack, F., & Merrill, R. (1995). Interhole correlations at Site 893, Santa Barbara Basin: Construction of a 16,000-year composite record using magnetic susceptibility and digital color imaging data. J. P. Kennett, J. G. Baldauf, & M. Lyle (Eds.), In *Proceedings of the Ocean Drilling Program, Scientific Results* (Vol. 146 (Pt 2), pp. 169–192). College Station, TX: Ocean Drilling Program. <https://doi.org/10.2973/odp.proc.sr.146-2.287.1995>
- Ransom, B., Shea, K. F., Burkett, P. J., Bennett, R. H., & Baerwald, R. (1998). Comparison of pelagic and nepheloid layer marine snow: Implications for carbon cycling. *Marine Geology*, *150*, 39–50. [https://doi.org/10.1016/S0025-3227\(98\)00052-8](https://doi.org/10.1016/S0025-3227(98)00052-8)
- Reimer, P. J., Bard, E., Bayliss, A., Beck, J. W., Blackwell, P. G., Ramsey, C. B., et al. (2013). IntCal13 and Marine13 radiocarbon age calibration curves 0–50,000 years cal BP. *Radiocarbon*, *55*(4), 1869–1887. https://doi.org/10.2458/azu_js_rc.55.16947
- Reimers, C. E., Lange, C. B., Tabak, M., & Bernhard, J. M. (1990). Seasonal spillover and varve formation in the Santa Barbara Basin, California. *Limnology and Oceanography*, *35*(7), 1577–1585. <https://doi.org/10.4319/lo.1990.35.7.1577>
- Ropelewski, C. F., & Halpert, M. S. (1989). Precipitation patterns associated with the high index phase of the Southern Oscillation. *Journal of Climate*, *2*(3), 268–284. [https://doi.org/10.1175/1520-0442\(1989\)0022.0.co;2](https://doi.org/10.1175/1520-0442(1989)0022.0.co;2)
- Ross, T., Lott, N., McCown, S., & Quinn, D. (1998). *The El Niño winter of '97–'98* (pp. 1–28). Asheville, NC: National Climatic Data Center.
- Sarmiento, J. L., & Sundquist, E. T. (1992). Revised budget for the oceanic uptake of anthropogenic carbon dioxide. *Nature*, *356*(6370), 589–593. <https://doi.org/10.1038/356589a0>
- Scalan, E., & Smith, J. (1970). An improved measure of the odd-even predominance in the normal alkanes of sediment extracts and petroleum. *Geochimica et Cosmochimica Acta*, *34*(5), 611–620. [https://doi.org/10.1016/0016-7037\(70\)90019-0](https://doi.org/10.1016/0016-7037(70)90019-0)
- Schimmelmann, A., Hendy, I. L., Dunn, L., Pak, D. K., & Lange, C. B. (2013). Revised 2000-year chronostratigraphy of partially varved marine sediment in Santa Barbara Basin, California. *GFF*, *135*(3–4), 258–264. <https://doi.org/10.1080/11035897.2013.773066>
- Schimmelmann, A., Lange, C. B., & Meggers, B. J. (2003). Palaeoclimatic and archaeological evidence for a 200-yr recurrence of floods and droughts linking California, Mesoamerica and South America over the past 2000 years. *The Holocene*, *13*(5), 763–778. <https://doi.org/10.1191/0959683603hl661rp>
- Schimmelmann, A., & Tegner, M. J. (1991). Historical oceanographic events reflected in $^{13}\text{C}/^{12}\text{C}$ ratio of total organic carbon in laminated Santa Barbara Basin Sediment. *Global Biogeochemical Cycles*, *5*(2), 173–188. <https://doi.org/10.1029/91gb00382>
- Schimmelmann, A., Zhao, M., Harvey, C. C., & Lange, C. B. (1998). A large California flood and correlative global climatic events 400 years ago. *Quaternary Research*, *49*(1), 51–61. <https://doi.org/10.1006/qres.1997.1937>
- Schlesinger, M. E., & Jiang, X. (1991). Climatic responses to increasing greenhouse gases. *Eos Transactions American Geophysical Union*, *72*(53), 597–593. <https://doi.org/10.1029/90EO00417>
- Schwarz, J. R., Walker, J. D., & Colwell, R. R. (1974). Deep-sea bacteria: Growth and utilization of hydrocarbons at ambient and in situ pressure. *Applied Microbiology*, *28*(6), 982–986. <https://doi.org/10.1128/aem.28.6.982-986.1974>
- Sigman, D. M., Robinson, R., Knapp, A. N., van Geen, A., McCorkle, D. C., Brandes, J. A., & Thunell, R. C. (2003). Distinguishing between water column and sedimentary denitrification in the Santa Barbara Basin using the stable isotopes of nitrate. *Geochemistry, Geophysics, Geosystems*, *4*(5), 1040. <https://doi.org/10.1029/2002GC000384>
- Smith, S. V., & Hollibaugh, J. T. (1993). Coastal metabolism and the oceanic organic carbon balance. *Reviews of Geophysics*, *31*(1), 75–89. <https://doi.org/10.1029/92RG02584>
- So, C. M., & Young, L. Y. (1999). Isolation and characterization of a sulfate-reducing bacterium that anaerobically degrades alkanes. *Applied and Environmental Microbiology*, *65*(7), 2969–2976. <https://doi.org/10.1128/aem.65.7.2969-2976.1999>
- Soutar, A., & Crill, P. A. (1977). Sedimentation and climatic patterns in the Santa Barbara Basin during the 19th and 20th centuries. *Geological Society of America Bulletin*, *88*(8), 1161. [https://doi.org/10.1130/0016-7606\(1977\)88<1161:sacpit>2.0.co;2](https://doi.org/10.1130/0016-7606(1977)88<1161:sacpit>2.0.co;2)
- Soutar, A., Kling, S. A., Crill, P. A., Duffrin, E., & Bruland, K. W. (1977). Monitoring the marine environment through sedimentation. *Nature*, *266*(5598), 136–139. <https://doi.org/10.1038/266136a0>
- Stallard, R. F. (1998). Terrestrial sedimentation and the carbon cycle: Coupling weathering and erosion to carbon burial. *Global Biogeochemical Cycles*, *12*(2), 231–257. <https://doi.org/10.1029/98GB00741>
- Sweeney, R. E., & Kaplan, I. (1980). Natural abundances of ^{15}N as a source indicator for near-shore marine sedimentary and dissolved nitrogen. *Marine Chemistry*, *9*(2), 81–94. [https://doi.org/10.1016/0304-4203\(80\)90062-6](https://doi.org/10.1016/0304-4203(80)90062-6)
- Tems, C. E., Berelson, W. M., & Prokopenko, M. G. (2015). Particulate $\delta^{15}\text{N}$ in laminated marine sediments as a proxy for mixing between the California Undercurrent and the California Current: A proof of concept. *Geophysical Research Letters*, *42*, 419–427. <https://doi.org/10.1002/2014gl061993>
- Thornton, S. E. (1984). Basin model for hemipelagic sedimentation in a tectonically active continental margin: Santa Barbara Basin, California Continental Borderland. *Geological Society, London, Special Publications*, *15*, 377–394. <https://doi.org/10.1144/GSL.SP.1984.015.01.25>
- Thornton, S. E. (1986). Origin of mass flow sedimentary structures in hemipelagic basin deposits: Santa Barbara Basin, California Borderland. *Geo-Marine Letters*, *6*(1), 15–19. <https://doi.org/10.1007/bf02311691>
- Thunell, R. C. (1998). Seasonal and annual variability in particle fluxes in the Gulf of California: A response to climate forcing. *Deep Sea Research Part I: Oceanographic Research Papers*, *45*(12), 2059–2083. [https://doi.org/10.1016/S0967-0637\(98\)00053-3](https://doi.org/10.1016/S0967-0637(98)00053-3)

- Thunell, R. C. (2003). Distinguishing between water column and sedimentary denitrification in the Santa Barbara Basin using the stable isotopes of nitrate. *Geochemistry, Geophysics, Geosystems*, 4(5), 1040. <https://doi.org/10.1029/2002gc000384>
- Thunell, R. C., Tappa, E., & Anderson, D. M. (1995). Sediment fluxes and varve formation in Santa Barbara Basin, offshore California. *Geology*, 23(12), 1083. [https://doi.org/10.1130/0091-7613\(1995\)023<1083:SFAVFI>2.3.CO;2](https://doi.org/10.1130/0091-7613(1995)023<1083:SFAVFI>2.3.CO;2)
- Voss, M., Dippner, J. W., & Montoya, J. P. (2001). Nitrogen isotope patterns in the oxygen-deficient waters of the Eastern Tropical North Pacific Ocean. *Deep Sea Research Part I: Oceanographic Research Papers*, 48(8), 1905–1921. [https://doi.org/10.1016/S0967-0637\(00\)00110-2](https://doi.org/10.1016/S0967-0637(00)00110-2)
- Wakeham, S. G., Hedges, J. I., Lee, C., Peterson, M. L., & Hernes, P. J. (1997). Compositions and transport of lipid biomarkers through the water column and surficial sediments of the equatorial Pacific Ocean. *Deep Sea Research Part II: Topical Studies in Oceanography*, 44(9–10), 2131–2162. [https://doi.org/10.1016/s0967-0645\(97\)00035-0](https://doi.org/10.1016/s0967-0645(97)00035-0)
- Waliser, D., & Guan, B. (2017). Extreme winds and precipitation during landfall of atmospheric rivers. *Nature Geoscience*, 10(3), 179–183. <https://doi.org/10.1038/ngeo2894>
- Wang, B., Yang, J., Jiang, H., Zhang, G., & Dong, H. (2019). Chemical composition of *n*-alkanes and microbially mediated *n*-alkane degradation potential differ in the sediments of Qinghai-Tibetan lakes with different salinity. *Chemical Geology*, 524, 37–48. <https://doi.org/10.1016/j.chemgeo.2019.05.038>
- Wang, Y., Hendy, I. L., & Thunell, R. (2019). Local and remote forcing of denitrification in the Northeast Pacific for the last 2000 years. *Paleoceanography and Paleoclimatology*, 34. <https://doi.org/10.1029/2019pa003577>
- Warrick, J. A., DiGiacomo, P. M., Welsberg, S. B., Nezlin, N. P., Mengel, M., Jones, B. H., et al. (2007). River plume patterns and dynamics within the Southern California Bight. *Continental Shelf Research*, 27(19), 2427–2448. <https://doi.org/10.1016/j.csr.2007.06.015>
- Warrick, J. A., & Farnsworth, K. L. (2009). Sources of sediment to the coastal waters of the Southern California Bight. In H. J. Lee & W. R. Normark (Eds.), *Earth science in the urban ocean: The Southern California Continental Borderland*, Geological Society of America Special Paper (Vol. 454, pp. 39–52). Geological Society of America. [https://doi.org/10.1130/2009.2454\(2.2\)](https://doi.org/10.1130/2009.2454(2.2))
- Warrick, J. A., Washburn, L., Brzezinski, M. A., & Siegel, D. A. (2005). Nutrient contributions to the Santa Barbara Channel, California, from the ephemeral Santa Clara River. *Estuarine, Coastal and Shelf Science*, 62(4), 559–574. <https://doi.org/10.1016/j.ecss.2004.09.033>
- Whyte, L. G., Hawari, J., Zhou, E., Luc, B., Inniss, W. E., & Greer, C. W. (1998). Biodegradation of variable-chain-length alkanes at low temperatures by a psychrotrophic *Rhodococcus* sp. *Applied and Environmental Microbiology*, 64(7), 2578–2584. <https://doi.org/10.1128/aem.64.7.2578-2584.1998>
- Wroblewski, J. S., & Richman, J. G. (1987). The non-linear response of plankton to wind mixing events—Implications for survival of larval northern anchovy. *Journal of Plankton Research*, 9(1), 103–123. <https://doi.org/10.1093/plankt/9.1.103>
- Young, L. Y., & Phelps, C. D. (2005). Metabolic biomarkers for monitoring *in situ* anaerobic hydrocarbon degradation. *Environmental Health Perspectives*, 113(1), 62–67. <https://doi.org/10.1289/ehp.6940>